

A Software Tool for Refocusing of Light Fields

by

Canyu Sun
B.Eng., Sichuan University, 2018

A Report Submitted in Partial Fulfillment
of the Requirements for the Degree of

MASTER OF ENGINEERING

in the Department of Electrical and Computer Engineering

© Canyu Sun, 2019
University of Victoria

All rights reserved. This report may not be reproduced in whole or in part, by photocopy
or other means, without the permission of the author.

Supervisory Committee

A Software Tool for Refocusing of Light Fields

by

Canyu Sun
B.Eng., Sichuan University, 2018

Supervisory Committee

Dr. Panajotis Agathoklis, Department of Electrical and Computer Engineering
Supervisor

Dr. Daniela Constantinescu, Department of Mechanical Engineering
Outside Member

Abstract

In this project, an interactive software tool is designed for volumetric refocusing of a light field (LF) by using a post-capture refocusing technique. This software tool aims to help people like traditional photographers who do not know LFs to understand what the refocus of LF is and how the bokeh is generated.

LF emerges as a technology allowing to capture richer visual information which is a higher dimensional representation of visual data. The spectral region of support (ROS) of a Lambertian point at a constant depth is shown to be two hyperfans in four-dimensional (4-D) frequency domain. Based on the spectral analysis, a 4-D finite-extent impulse response (FIR) hyperfan filter is designed for refocusing of the LF. Two filter parameters can be changed to result in different visual effect of the refocused images, namely α and θ . Experiments are conducted to evaluate the effect of these two parameters by using LFs of different size. Comparisons and analyses are made using different LFs and different parameters. Based on these comparisons, conclusions are drawn about the effect of fan filters on the quality of the refocused images. It is found that filter parameter α controls the depth of the focal plane and θ controls the depth of field (DOF) of the refocused image.

Furthermore, the structure of the software and the design of each function is described. The software can be used to display a LF as a video, display the center image of the LF, display the refocused image and the figure of the filter used as well as extracting central images of the LF. The interactive user interface makes the refocusing of LFs easier.

Table of Contents

Supervisory Committee	ii
Abstract	iii
Table of Contents	iv
List of Acronym	vi
List of Figures	vii
Acknowledgments	ix
Dedication	x
Chapter1 Introduction	1
1.1 Objective	1
1.2 LF	1
1.3 Bokeh	2
1.3.1 Background of Bokeh	3
1.4 Report Outline	4
Chapter2 Theory	5
2.1 Geometrical Optics and Relation between Bokeh	5
2.1.1 Focus	5
2.1.2 Focal Plane	5
2.1.3 Point Spread Function (PSF) and Circle of Confusion (COC)	7
2.1.4 DOF	8
2.1.5 Visual Effects of Bokeh	8
2.2 LF	10
2.2.1 LF Reresentation	10
2.2.2 Two-plane Parameterization	11
2.2.3 Epipolar Geometry	11
2.3 The Spectral ROS of a LF	12
2.4 Connection between LFs and Bokeh	16
2.5 Summary	16
Chapter3 Comparison and Analysis	17
3.1 Proposed 4-D FIR Hyperfan Filter	17
3.2 Design of 4-D FIR Hyperfan Filter	18
3.2.1 Coefficients of $Hxu(\mathbf{z})$ and $Hyv(\mathbf{z})$	18
3.2.2 Selection of the 2-D Window Functions	19
3.3 LF Dataset	19
3.4 Effect of Alpha	20
3.5 Effect of the angle θ (Opening) of Fan Filter	22
3.6 Additional Examples	23
3.6.1 LF Data of size $15 \times 15 \times 434 \times 625 \times 4$	23
3.6.2 LF Data of size $9 \times 9 \times 512 \times 512 \times 3$	25
3.7 Discussion	28
3.8 Summary	28
Chapter4 Software Design	29
4.1 Specification and Structure	29
4.2 Interface Design	29
4.3 LF Display as a Video	33
4.4 Extract and Store the LF Images	34

4.5	Volumetric Refocusing	35
4.6	Summary	38
Chapter5	Conclusions and Future Work	39
5.1	Conclusions.....	39
5.2	Future Work.....	39
Reference	40
Appendix A	Function List of Software Tool	42
Appendix B	Derivation of the Spectrum of a Lambertian Point Source at a Constant Depth.....	43

List of Acronym

2-D	Two-Dimensional
3-D	Three-Dimensional
4-D	Four-Dimensional
DOF	Depth of Field
FFT	Fast Fourier Transform
FIR	Finite-extent Impulse Response
GUI	Graphical User Interface
IIR	Infinite-extent Impulse Response
LF	Light Field
ROS	Region of Support

List of Figures

Figure 1.1 Multiview of LF Data "dishes"[8].....	2
Figure 1.2 A Night View Containing Bokeh[9].....	2
Figure 1.3 Explanation for Photography about Bokeh[11].....	3
Figure 2.1 Focus of the Lens[19].....	5
Figure 2.2 Illustration of Lens Equation.....	6
Figure 2.3 Explanation for Photography Focal Plane[11].....	7
Figure 2.4 An Example of PSF[21].....	7
Figure 2.5 Projection of a Point on Image Plane of Different Distance.....	8
Figure 2.6 Photograph with Bokeh[22].....	9
Figure 2.7 Bokeh as the Subject[13].....	9
Figure 2.8 5-D Plenoptic Function Representation.....	10
Figure 2.9 Two-Plane Parameterization.....	11
Figure 2.10 Epipolar Geometry.....	12
Figure 2.11 Two-Plane Parameterization of a Lambertian Point[29].....	13
Figure 2.12 The Representation of a Lambertian Point Source in the xu Subspace[29]..	13
Figure 2.13 ROS of the Spectrum of a Lambertian Point Source 1[29].....	15
Figure 2.14 ROS of the Spectrum of a Lambertian Point Source 2[29].....	16
Figure 3.1 The spectral ROS of a Lambertian object and the passband of the 4-D hyperfan filter $H(z)$ in the $\omega_x\omega_u$ subspace.....	17
Figure 3.2 The ROS of the Spectrum and the passband of the 4-D hyperfan filter $H(z)$ in the $\omega_x\omega_u$ subspace and $\omega_y\omega_v$	18
Figure 3.3 Center Image of LF "University" (left) and "Magnet"(right).....	19
Figure 3.4 Most Centered Image of LF "Dishes" (left) and "Ankylosaurus and Diplodocus"(right).....	20
Figure 3.5 Refocused LF Image for Different α	21
Figure 3.6 Refocused LF Image with Different α	21
Figure 3.7 Refocused LF Image with Different θ	22
Figure 3.8 Magnitude Response of Hyperfan Filter with $\alpha = 90$ and $\theta = 10$	23
Figure 3.9 Refocused LF Image with Different α	24
Figure 3.10 Refocused LF Image with Different θ	25
Figure 3.11 Refocused LF Image for Different α	26
Figure 3.12 Refocused LF Image for Different θ	27
Figure 4.1 Software Tool Functional Block Diagram.....	29
Figure 4.2 Functional Block Diagram of GUI Module.....	29
Figure 4.3 Start to Design a Layout for GUI.....	30
Figure 4.4 Screenshot of Opening GUI Guide.....	30
Figure 4.5 Screenshot of GUI Design.....	31
Figure 4.6 Screenshot of GUI.....	31
Figure 4.7 Screenshot of Size-adaptable GUI.....	32
Figure 4.8 Flow Diagram of LF Display Module.....	33
Figure 4.9 LF Display.....	34
Figure 4.10 Flow Diagram of Extract and Store of LF Images Module.....	34
Figure 4.11 Screenshot of $N \times N$ Images of LF.....	35
Figure 4.12 Flow Diagram of Volumetric Refocusing Module.....	36

Figure 4.13 File Selector 37
Figure 4.14 Refocusing of LF 37
Figure 4.15 Screenshot of Fully Running Program 38

Acknowledgments

There goes an old saying in China, “Day as a teacher, like fatherhood”.

First, I would like to express my deepest gratitude to my supervisor, Dr. Pan Agathoklis. I am thankful to Dr. Pan Agathoklis for all the inspiring meetings and discussions and his efforts to lead me to think what is important and tell me how to achieve it. Not only the guidance of academic life, but also the mentorship of life. He encouraged me that life is hard and that is what a man has to go through during my hard time. My gratitude to him is beyond words. Without the support and guidance from him, I would not be able to be here. Besides those, I respect and admire his endless commitment and dedication to the field of multidimensional signal processing.

Then, I would like to thank my girlfriend, Zhaoxin Liu. Without your encouragement and understanding, I would never conquer the difficulties in my daily life. Thank you for your companion and caring day and night.

Next, I take this chance to express my heartfelt thanks to all my family members for their constant support, encouragement and unconditional love. And thanks for the help and companion from my classmates, roommates and four faithful pals from China.

Also, I would like to express my thankfulness to the course instructors Dr. Wu-sheng Lu, Dr. T. Aaron Gulliver, Dr. Hong-chuan Yang, Dr. Xiao-dai Dong, for their outstanding teaching and inspiration.

Finally, I want to thank UVic for providing me the opportunity to study here and a chance to experience the life in Victoria.

Dedication

To schools
Renmin Primary School
and
Bashu Middle School
where I received my primary and secondary education, respectively,
and
to *Sichuan University*
where I received higher education.

Chapter1 Introduction

1.1 Objective

The objective of the project is to develop a software tool for post-capture refocusing of LFs. This tool is based on the theory of refocusing LFs by developing appropriate filters in the 4D frequency domain. By varying the filter parameters, the user can change the focal plane depths and DOF and observe the resulting images. Processing of LF in the frequency domain is a new technology that enables applications such as refocusing, depth filtering etc. which cannot be done by traditional 2-D photography. A new Graphical User Interface (GUI) for this tool is developed with an easy-to-use interface and visualization to help users observing how the parameters of the filter affect the visual effect of the image and in particular how focal depth, DOF and/or bokeh are varied.

1.2 LF

Light plays a vital role in our daily life while we communicate with the world around us. But while the world is made of objects, these objects do not communicate their properties directly to an observer; they rather fill the space around them with a pattern of light rays that is perceived and interpreted by the human visual system. Such a pattern of light rays can be measured, yielding the now ubiquitous images and videos. Thus, the concept of LF arises. Also, the LF image and LF video have developed since then.

To put it in a simple way, just like the concept of magnetic field and electric field, the LF is a field that consists of the total light rays in three-dimensional (3-D) space, flowing through every point and in every direction. Everything we can see is illuminated by light coming from a light source (e.g. the sun), travelling through space and hitting surfaces. Then, at each surface, light is partly absorbed and partly reflected to another surface and finally reaches our eyes. What can be seen depends on the position in LFs. By moving around, they can be perceived and used to get the relative position of objects in the environment.

LF imaging [1] and processing has emerged as a technology allowing to capture richer visual information from our world. As opposed to traditional photography, which captures a 2-D projection of the light in the scene integrating the angular domain, LFs collect radiance from rays in all directions, demultiplexing the angular information lost in conventional photography.

This higher dimensional representation of visual data offers powerful capabilities [2] for scene understanding and substantially improves the performance of traditional computer vision problems such as depth sensing, post-capture refocusing, segmentation, video stabilization, material classification, reflectance and shape estimation [3] etc. On the other hand, the high dimensionality of LFs also brings up new challenges [4] in terms of data capture, data compression [5], content editing, and display. Taking these two elements together, research in LF image processing has become increasingly popular in the computer vision, computer graphics, and signal processing communities.

One way to capture LF was developed by Stanford University [6]. It uses a camera array made up of 96 cameras in different angle. Also there used to be a company designing the camera called Lytro [7] which can capture LFs.

The figure 1.1 displays the 5x5 central images of LF data “dishes” sequence from the Heidelberg dataset [8] which was stored as $9 \times 9 \times 512 \times 512$.

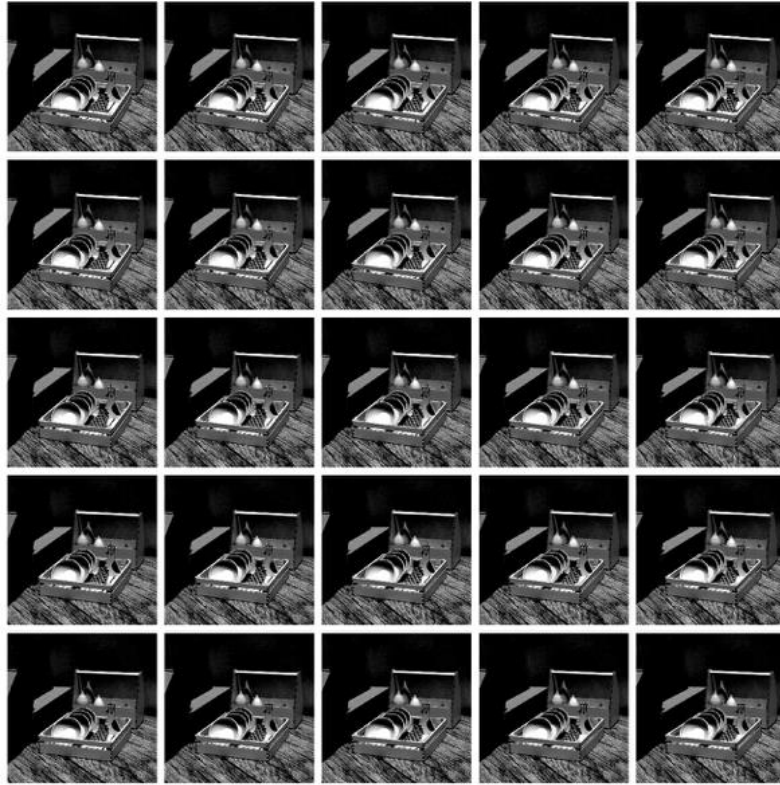


Figure 1.1 Multiview of LF Data "dishes"[8]

1.3 Bokeh

In photography, bokeh has been defined as “the way the lens renders out of focus points of light” [10]. An example of an image having bokeh background is shown below.

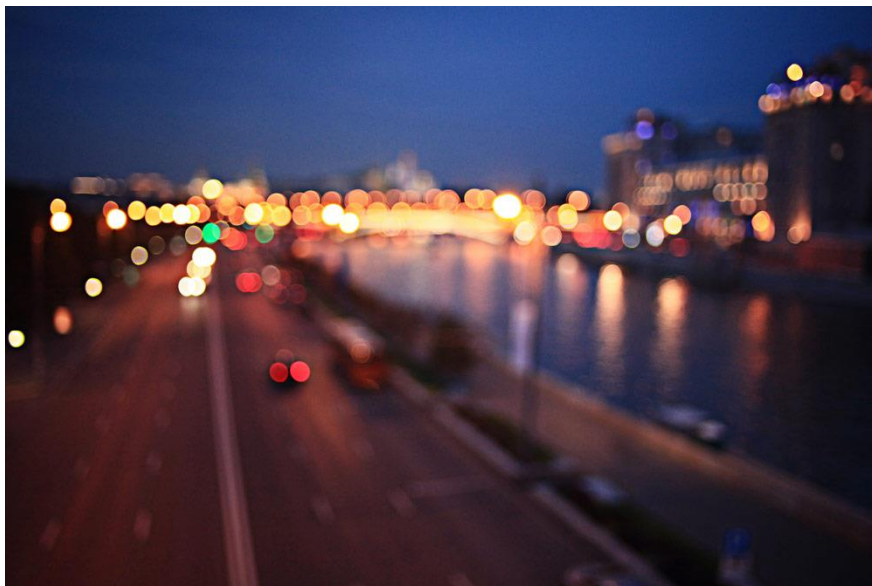


Figure 1.2 A Night View Containing Bokeh[9]

The following figure clearly illustrates in which area the bokeh is generated. For a camera lens, there is a focal plane so that objects which are at a certain distance are completely in focus. Objects outside the focal plane are not exactly in focus. However, there is a region that they can still be seen clearly called DOF which is denoted as “area of acceptable focus” in the figure below. If objects are located out of this range, then they will appear blurred which is called bokeh. The detail of how bokeh is generated will be introduced in the next chapter.

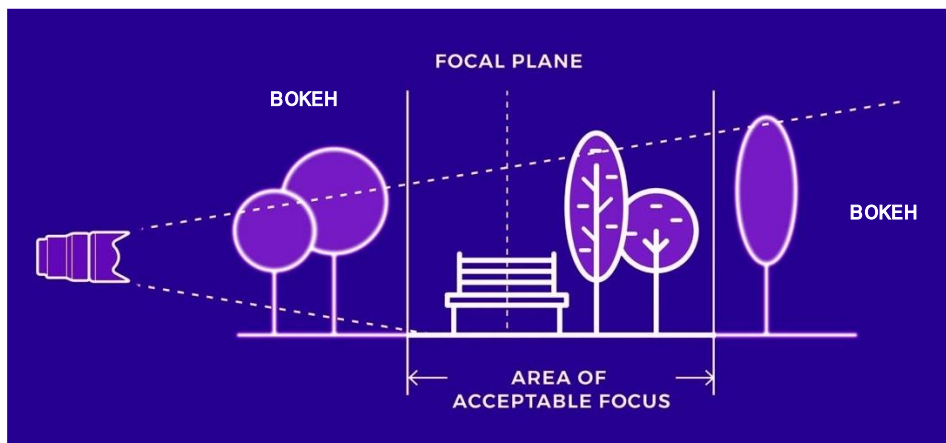


Figure 1.3 Explanation for Photography about Bokeh[11]

1.3.1 Background of Bokeh

Before the term “bokeh” came out, there were many discussions about the aesthetics of the out-of-focus specular highlights of a photograph [12], but until 1997, there wasn’t an appropriate word in English to describe the phenomenon.

The word “bokeh” was introduced to the photography world by Photo Techniques magazine in 1997. It is original from the Japanese word boke, which means “haze” or “blur”, the “blur quality”. Because of the dual meaning, we can say, “That photo has bokeh,” and we can also say, “That image has very pleasant bokeh.” The translation of those two statements is, “That photograph has specular highlights that are not in focus,” and “The out-of-focus areas of this photograph are pleasing to the eye.”[13].

Nikon, one of the most famous camera manufactures defines bokeh as “the effect of a soft out-of-focus background that you get when shooting a subject, using a fast lens, at the widest aperture [14], such as $f/2.8$ or wider”. For a simpler definition, bokeh is the pleasing or aesthetic quality of out-of-focus blur in a photograph.

In 2016, Apple Inc. released the iPhone 7 Plus which can take pictures with "Portrait Mode" (a bokeh like effect).[15] Samsung's Galaxy Note 8 has a similar effect available. Both phones use dual cameras to detect edges and create a "depth map" of the image, which the phones use to blur the out-of-focus portions of the photo. Other phones, like the Google Pixel, only use a single camera and machine learning to create a depth map [16].

In 2017, Vivo released a smartphone with dual front lenses for selfies with bokeh. The first, a 20 MP lens, uses a $1/2.78$ " sensor with $f/2.0$ aperture, while the second, an 8 MP $f/2.0$ lens, captures depth information. Bokeh can be made with a combination of

both lenses, and shots can be refocused even after they are captured, adding bokeh effects with different depths [17].

1.4 Report Outline

In chapter 1, some basic concepts and the objective of this project are presented. Then, the concepts of LF, LF imaging and processing and LF applications are introduced followed by presenting an example of LF. Next, the concept of bokeh and its applications are introduced as well as examples of photographs containing bokeh.

In chapter 2 some basic knowledge about geometrical optics like focus, focal plane, circle of confusion and DOF are provided which helps understand the theory of how bokeh is generated. Then, two representations of LFs are introduced to help understand the representation of LFs in 4-D frequency domain. At the end of this chapter, the connection between bokeh and LF is explained.

In chapter 3, the design of 4-D FIR hyperfan filters for volumetric refocusing is presented. This is followed by the introduction of the LF dataset used in the project and the structure of LF data. Then comparisons and analyses are made using different filter parameters and different LFs. At last, a discussion about the analyses and comparisons is presented.

In chapter 4, a software tool which can be used for post-capture refocusing is presented. It can be used to do refocusing, display a LF and refocused image as well as to extract central images of a LF. In this chapter, the structure of the software and the design of each function are described.

In chapter 5, a summary of the whole project and suggestions for the future work are presented.

Chapter2 Theory

In this chapter, some basic properties about geometrical optics are presented to explain the generation of LF images. Then LFs are analyzed in the 4-D frequency domain based on the work in [29] and the relationship between DOF, bokeh and 4-D spectrum of LF is explained.

2.1 Geometrical Optics and Relation between Bokeh

Geometrical optics is widely studied and useful in many engineering areas. They describe light propagation, assuming that light travels as rays. To analyze the theory behind the generation of bokeh, some terms from geometrical optics will be introduced and explained in the following sections.

2.1.1 Focus

The camera is a light-tight box that is used to expose a photosensitive surface (film or digital sensor) to light. In order to focus the light into a point on a surface, most cameras (and our own eyes) use a lens to direct the light.

For a lens, focal point F is a point onto which collimated light parallel to the axis is focused. Since light can pass through a lens in either direction, a lens has two focal points, one on each side. The distance in air from the lens to the focus is called the focal length f [18].

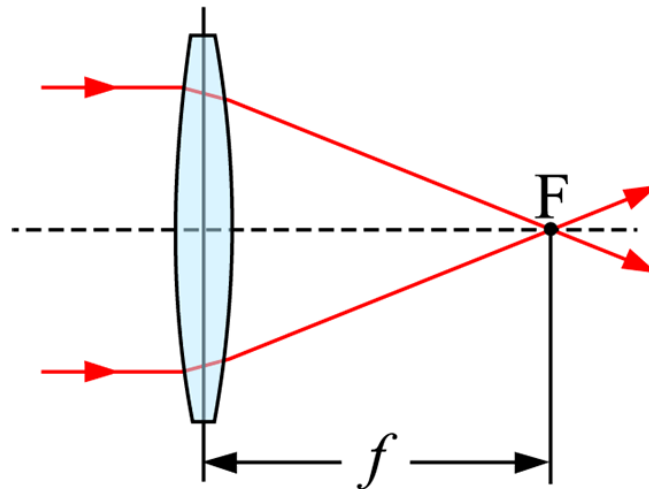


Figure 2.1 Focus of the Lens[19]

As figure shown above, F is the focal point and f is the focal length. Different lenses converge light at different focal points, and thus, have different focal lengths.

2.1.2 Focal Plane

The camera is designed to act similarly to a human eye [20]. As images are captured and transferred into digital images or film, so are images processed and converted into pictures inside the human eye. As a camera shutter adjusts to let in more or less light, so does the iris. One of the most fascinating aspects of the human eye is its ability to focus

on one part of a scene and block out distractions. By adjusting the focal plane and DOF on a camera, a photographer can create a similar selective-focusing effect.

It is important to understand how a 2-D image is generated by a single lens before moving on to $N \times N$ array of cameras generating 4-D LFs.

For a thin lens, the relation between the focal length f and the distance between object to the lens is given by the lens equation below.

$$\frac{1}{f} = \frac{1}{p} + \frac{1}{p'} \quad (2.1)$$

where f is focal length, p is the distance from the object to the length, p' is the distance from the image plane to the lens. Illustration of lens equation is shown below.

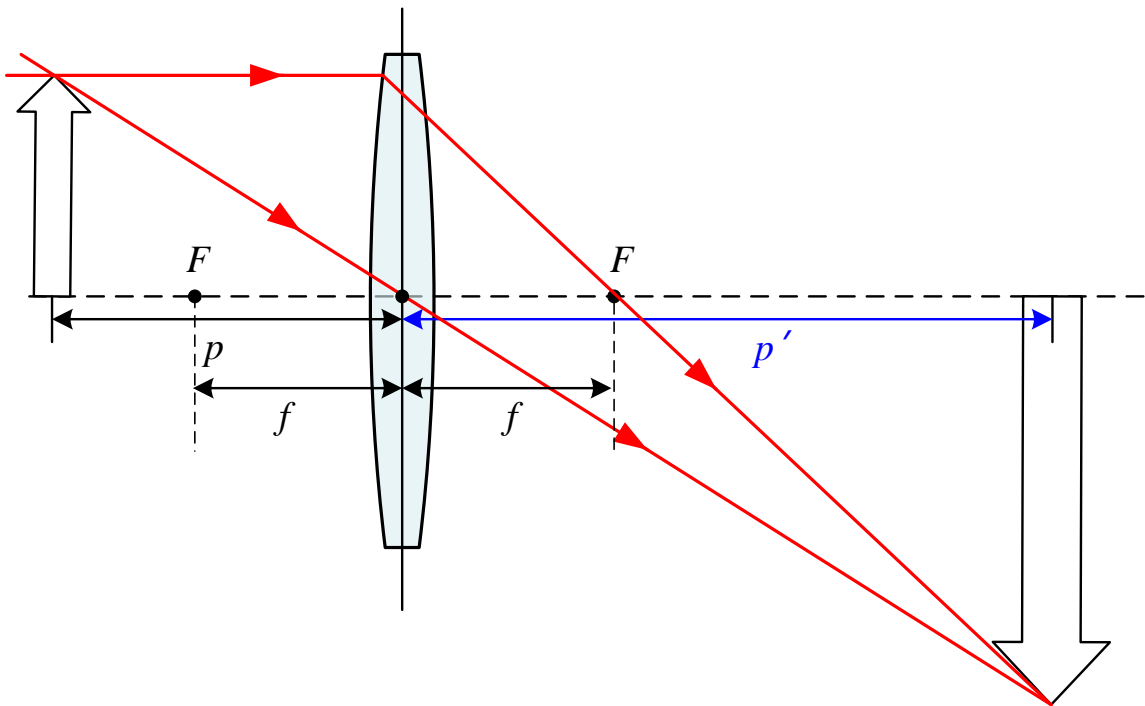


Figure 2.2 Illustration of Lens Equation

The focal plane is located at the distance between the perfect point of focus in an image and the camera lens. It is an area located at a certain distance in front of the camera lens. Despite what the name suggests, the focal plane, or the sharpest plane of focus in an image is not the only part of an image that appears to be in focus. Although the points adjacent to the focal plane are not in perfect focus, the brain registers them as being in focus if they lie within a certain range.

The area around the plane of focus that appears to be in focus is called the DOF [11] which will be introduced in the following section. The DOF can be adjusted to be deeper (more of the image appears in focus) or shallower (less of the image appears in focus) by adjusting the aperture (f-stop), the part of the camera that controls light entry.

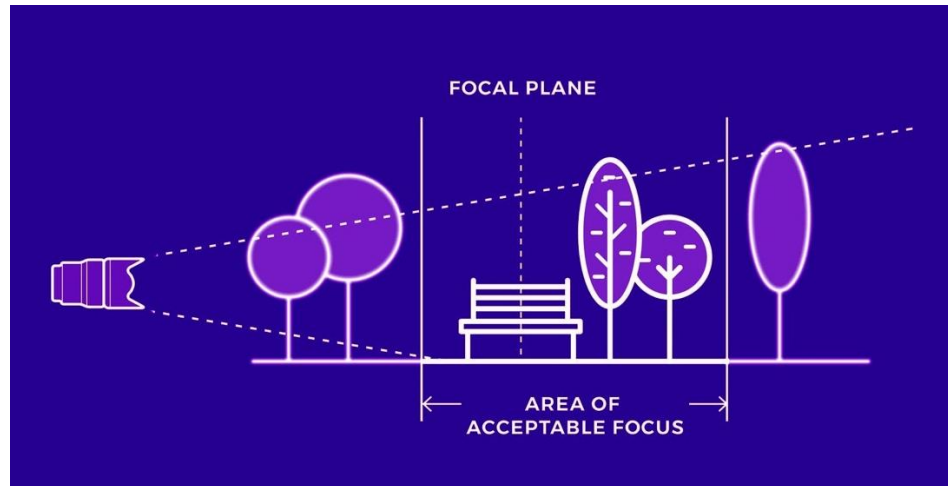


Figure 2.3 Explanation for Photography Focal Plane[11]

2.1.3 Point Spread Function (PSF) and Circle of Confusion (COC)

In engineering aspect, compared with human eyes, lenses are not perfect optical system. Therefore, when an input (i.e. visual stimuli) is passed through a lens, the input suffers a certain degree of deterioration. This degree of deterioration can be described by the PSF. PSF is the impulse response to a point source from an imaging system.

It is easy to imagine what is a PSF having a small dot of light and projecting it through a lens. The image of this point will not be the same, because the lens introduces a small amount of blur.

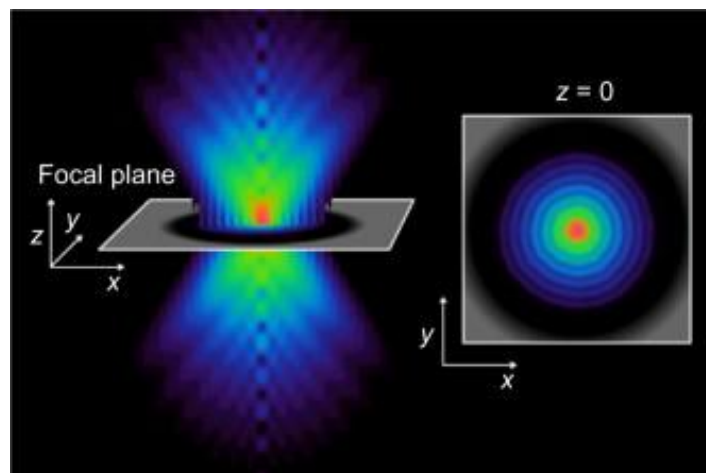


Figure 2.4 An Example of PSF[21]

In figure 2.4, cross-section of a 3-D PSF at $y = 0$ is shown on the left and top of the same slice and the focal plane ($z = 0$) is shown on the right. Ideally, without deterioration, only the red part would appear. In reality, the relative intensity of the light ray is decreased from the center. When changing the focal plane, we can see how the blurred part of the PSF increases which gives the COC in different depth.

The COC [23] is defined as the size of the largest blur spot that still appears as a single point (in focus) in an image. When the focus and the focal plane do not meet, a

point source of light (a round light source) appears bigger and no longer appears to be in sharp focus. In optics, a COC is an optical spot caused by a cone of light rays from a lens not coming to a perfect focus when imaging a point source. In photography, the COC is used to determine the DOF, the part of an image that is acceptably sharp.

2.1.4 DOF

It is defined as the area in an image, forward and aft of the focal plane, which also appears to be in focus in the image [13]. When you pass light through a lens and focus that light to form an image on a piece of film, digital sensor, projection screen, etc., the area of the image that is in true focus is very narrow—the focal plane, as shown in figure 2.5. Everything else is out of focus, to a certain degree. When portions of the foreground and background are outside of the DOF of the lens, the light that reflects from objects in those regions will be reproduced as circles at the image plane.

When a point of light is at the focal plane (middle illustration), it is reproduced as a point of light at the image plane. If the point is forward or aft of the focus plane, it is reproduced as a circle which is the COC introduced in section 2.1.3.

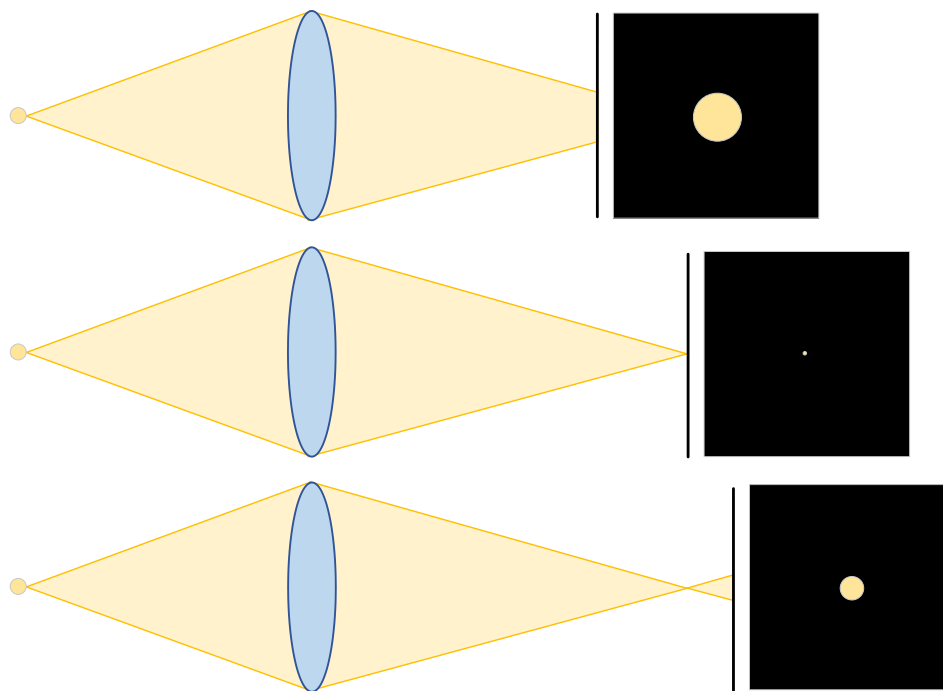


Figure 2.5 Projection of a Point on Image Plane of Different Distance

Depending on how the lens elements are designed and how the aperture of the lens is shaped, the bokeh will have distinct characteristics. These characteristics will, in general, do one of three things: complement the image, have no effect in the quality of the image, or distract from the subject. Interpretations on the effect of the out-of-focus areas of an image to the aesthetic quality of the image are as subjective as the photograph itself.

2.1.5 Visual Effects of Bokeh

One reason for people's obsession with bokeh is the fact that human eye, due to its excellent DOF, it cannot generate bokeh which exists in motion pictures or photographs.

Therefore, appropriate bokeh in photographs is a unique visual experience which is only able to be generated by viewing an image captured through an optical lens.



Figure 2.6 Photograph with Bokeh[22]

To create visible bokeh in the photographs, it can be done by increasing the distance between the subject and the background. Alternatively, it can also be done by decreasing the distance between the camera and subject. The shallower the depth-of-field, or further the background is, the more out-of-focus it will be. Highlights located at the background will show more visible bokeh too.

In general, bokeh can be the whole or part of the subject in a photograph and can be used by the photographers to convey more than the image of the object.



Figure 2.7 Bokeh as the Subject[13]

2.2 LF

2.2.1 LF Reresentation

Light is a fundamental form of conveying information. The concept of LF was initially created by Gershun [24]. The LF is a vector function that describes the amount of light flowing in every direction through every point in space. The light rays emanating from a scene is completely described by the seven-dimensional (7-D) plenoptic (derived by combining the Latin term *plenus* with the term optic) function, proposed in [25]. The 7-D plenoptic function [26] describes the intensity of light rays passing through the center of an ideal camera at every possible location in the 3-D space (x, y, z) , at every possible angle (θ, ϕ) , for every wavelength λ and at every time t . The function can be formulated as follows:

$$P(\theta, \phi, \lambda, t, x, y, z) \quad (2.2)$$

Generally, the 7-D plenoptic function describes the light rays in a scene as a function of time, spectral content, orientation and position. The plenoptic illumination function is an idealized function used in computer vision and computer graphics to express the image of a scene from any possible viewing position at any viewing angle at any point in time. It is not being used in practice but is conceptually useful in understanding other concepts in vision and graphics.

There is a simplified version [27] of plenoptic function with 5 dimensions by assuming a constant wavelength and time so that two dimensions can be eliminated. Then, the space of all possible light rays is given by the five-dimensional plenoptic function, and the magnitude of each ray is given by the radiance. The function can be formulated as follows:

$$P(\theta, \phi, x, y, z) \quad (2.3)$$

The 5-D plenoptic function of LFs is visualized as below.

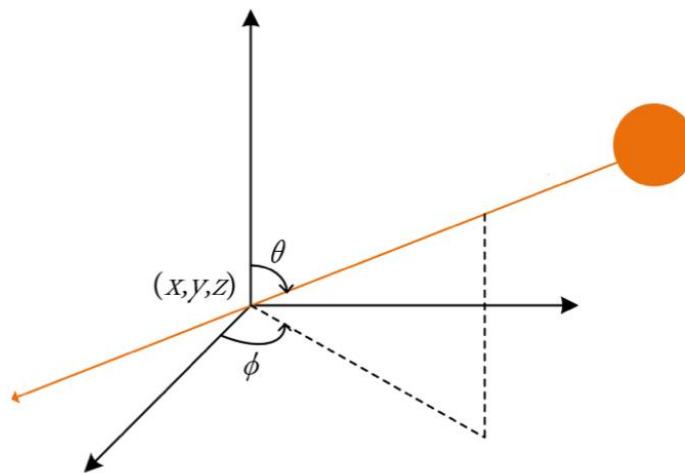


Figure 2.8 5-D Plenoptic Function Representation

Assuming constant intensity along the ray we can represent a ray using two-plane parameterization presented in the next section.

2.2.2 Two-plane Parameterization

One of the methods to describe a LF is the simplified 4-D function in free space. It needs only 4 parameters to describe LFs by considering only the color of each ray as a function of its position and orientation in a static scene, and by limiting each ray to have same value at every point along its direction of propagation. Thus, there is a great reduction of data required to represent a LF. One of the most common representation is the two-plane parameterization [6] shown below.

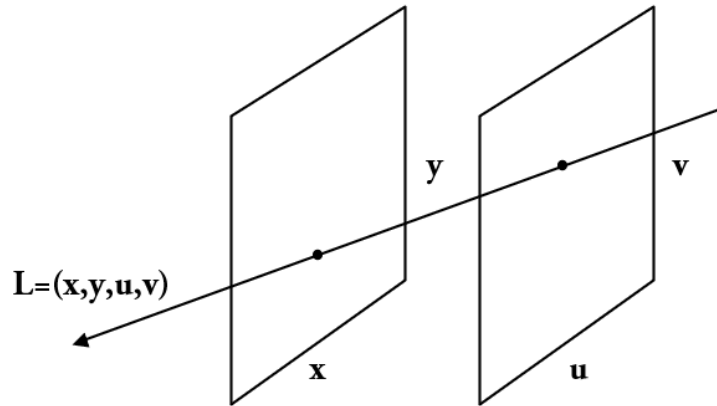


Figure 2.9 Two-Plane Parameterization

While this parameterization cannot represent all rays, for example rays parallel to the two planes if the planes are parallel to each other, it has the advantage of relating closely to the analytic geometry of perspective projection. Indeed, a simple way to think about a two-plane LF is as a collection of perspective images of the xy plane (and any objects that may lie astride or beyond it), each taken from an observer position on the uv plane.

2.2.3 Epipolar Geometry

Epipolar plane is an alternative method to represent light rays[28]. It is included here for completeness, since the analysis in the 4-D frequency domain will be based on the two-plane parameterization.

The figure 2.10 depicts two pinhole cameras O_L and O_R looking at point X . In real cameras, the image plane is behind the focal plane, and produces an image that is symmetric about the focal plane of the lens. Here, the problem is simplified by placing a virtual image plane in front of the focal center (i.e. optical center) of each camera lens to produce an image not transformed by the symmetry. O_L and O_R represent the centers of symmetry of the two cameras lenses. X represents the point of interest in both cameras. Points X_L and X_R are the projections of point X onto the image planes[28].

Each camera captures a 2-D image of the 3-D world. This conversion from 3-D to 2-D is referred to as a perspective projection and is described by the pinhole camera model. It is common to model this projection operation by rays that emanate from the camera,

passing through its focal center. Note that each emanating ray corresponds to a single point in the image.

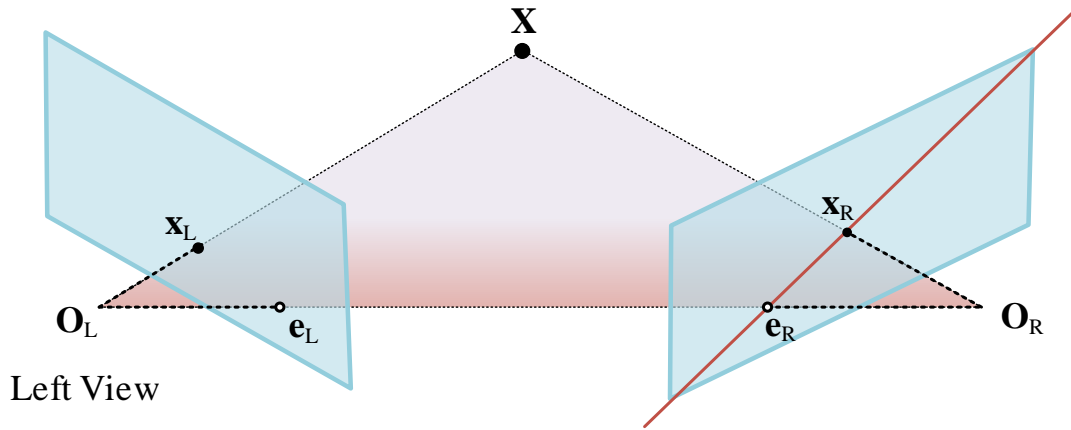


Figure 2.10 Epipolar Geometry

2.2.3.1 Epipolar Point

Since the optical centers of the camera's lenses are distinct, each center projects onto a distinct point into the other camera's image plane. These two image points, denoted by e_L and e_R , are called epipolar points[28].

2.2.3.2 Epipolar Line

The line O_L-X is seen by the left camera as a point because it is directly in line with that camera's lens optical center. However, the right camera sees this line as a line in its image plane. That line (e_R-x_R) in the right camera is called an epipolar line. Symmetrically, the line O_R-X seen by the right camera as a point is seen as epipolar line e_L-x_L by the left camera[28].

2.2.3.3 Epipolar Plane

As an alternative visualization, consider the points X , O_L and O_R that form a plane called the epipolar plane. The epipolar plane intersects each camera's image plane where it forms lines—the epipolar lines. All epipolar planes and epipolar lines intersect the epipolar point regardless of where X is located[28].

2.2.3.4 Epipolar Plane Image (EPI)

Since the points on an epipolar plane are projected onto one line in each image, all the information about them is contained in that sequence of lines. To concentrate this information in one place, we constructed an image from this sequence of lines. We named this image an EPI because it contains all the information about the features in one epipolar plane[28].

2.3 The Spectral ROS of a LF

The analysis of LF in 4-D frequency domain is mainly based on work in [29]. The two representations of LF introduced in section 2.2.2 and 2.2.3 correspond to time/space domain while this section focused on the frequency domain. The spectral ROS of a

Lambertian object is introduced below. To this end, we consider the standard two-plane parameterization of light rays emanating from a Lambertian object as shown in figure 2.11.

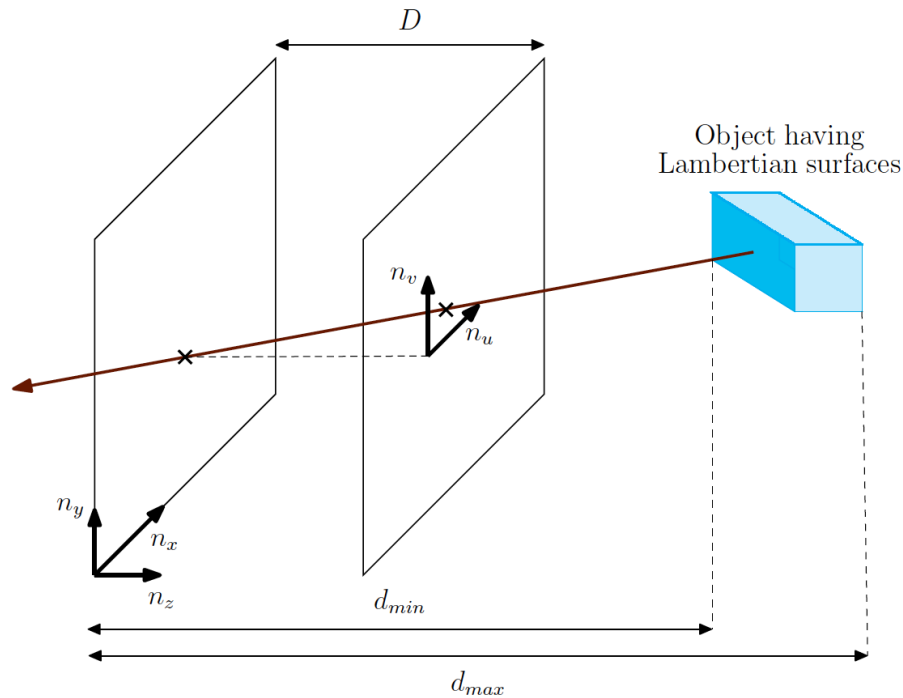


Figure 2.11 Two-Plane Parameterization of a Lambertian Point[29]

Here, coordinates $(n_x, n_y) \in \mathbb{Z}^2$ stand for the camera plane and $(n_u, n_v) \in \mathbb{Z}^2$ parameterize the focal plane. The distance between camera plane and focal plane is a constant denoted by D . To derive the spectral ROS of a LF corresponding to a Lambertian object, the Lambertian object is modeled as a collection of Lambertian point sources [29] located in the depth range $z_0 \in [d_{min}, d_{max}]$.

To have a top view of the two-plane parameterization above, we get the following figure.

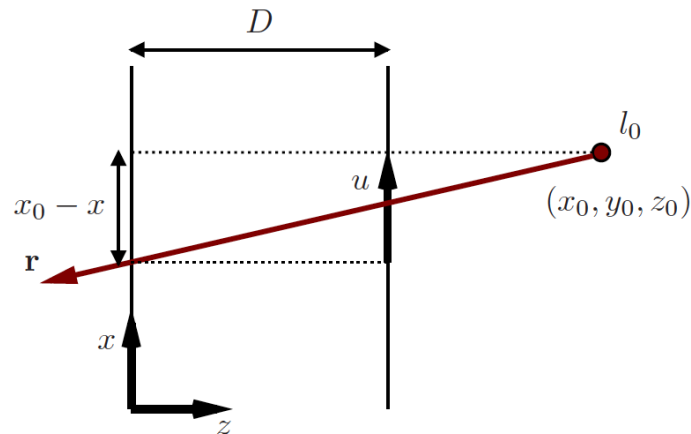


Figure 2.12 The Representation of a Lambertian Point Source in the xu Subspace[29]

According to the triangle geometry, it is easy to know that

$$\frac{x_0 - x}{u} = \frac{z_0}{D} \quad (2.4a)$$

Then we have

$$mx + u + c_x = 0 \quad (2.4b)$$

Where

$$m = \frac{D}{z_0} \quad (2.4c)$$

$$c_x = \frac{-Dx_0}{z_0} \quad (2.4d)$$

Which is the same for the subspace yv . According to [29], we have:

$$mx + u + c_x = 0 \quad (2.5a)$$

$$my + v + c_y = 0 \quad (2.5b)$$

Where

$$m = \frac{D}{z_0} \quad (2.5c)$$

$$c_x = \frac{-Dx_0}{z_0} \quad (2.5d)$$

$$c_y = \frac{-Dy_0}{z_0} \quad (2.5e)$$

The set of points that satisfies both equations above belongs to a plane defined by the intersection of these two hyperplanes. This plane is exactly the solution of the two equations above. Only points belonging to this plane of intersection correspond to rays emanating from the point source with all other points in the LF have a value of zero.

Here, the Lambertian point source is represented as a plane of constant value l_0 (intensity) in the corresponding 4-D continuous domain LF $l_{4C}(x, y, u, v)$. The 4-D continuous domain LF signal is denoted by l_{4C} . Its spectrum is denoted by L_{4C} . When analyzing only one point, the ROS of this point is denoted by \mathcal{P} and the ROS of an object is denoted by \mathcal{O} . Thus, the LF $l_{4C}(x, y, u, v)$ [29] can be expressed as:

$$l_{4C}(x, y, u, v) = l_0 \delta(mx + u + c_x) \delta(my + v + c_y) \quad (2.6)$$

Where $\delta(\cdot)$ is 1-D continuous-domain impulse function.

The spectrum of $l_{4C}(x, y, u, v)$, $L_{4C}(\Omega_x, \Omega_y, \Omega_u, \Omega_v)$ can be obtained [30] as:

$$L_{4C}(\Omega_x, \Omega_y, \Omega_u, \Omega_v) = 4\pi^2 l_0 \delta(\Omega_x - m\Omega_u) \delta(\Omega_y - m\Omega_v) e^{j(\Omega_u c_x + \Omega_v c_y)} \quad (2.7)$$

Where $(\Omega_x, \Omega_y, \Omega_u, \Omega_v) \in \mathbb{R}^4$.

The ROS \mathcal{P}_{4C} of the spectrum $L_{4C}(\Omega_x, \Omega_y, \Omega_u, \Omega_v)$ [29] can be obtained from the formula above as:

$$\mathcal{P}_{4C} = \mathcal{H}_{4C,xu} \cap \mathcal{H}_{4C,yv} \quad (2.8)$$

Where

$$\mathcal{H}_{4C,xu} = \{(\Omega_x, \Omega_y, \Omega_u, \Omega_v) \in \mathbb{R}^4 | \Omega_x - m\Omega_u = 0\} \quad (2.9a)$$

$$\mathcal{H}_{4C,yv} = \{(\Omega_x, \Omega_y, \Omega_u, \Omega_v) \in \mathbb{R}^4 | \Omega_y - m\Omega_v = 0\} \quad (2.9b)$$

$\mathcal{H}_{4C,xu}$ is the subspace of Ω_u, Ω_x and $\mathcal{H}_{4C,yv}$ is the subspace of Ω_v, Ω_y of support region in frequency domain for a fixed α :

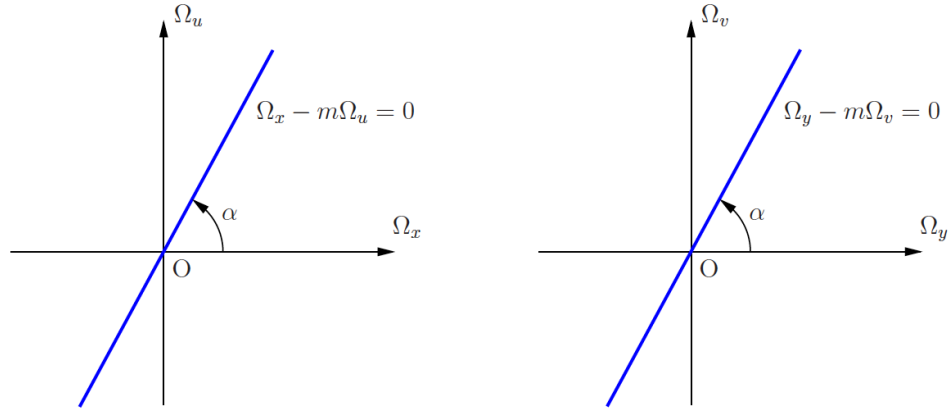


Figure 2.13 ROS of the Spectrum of a Lambertian Point Source 1[29]

Figure 2.13 is a plane through the origin in the 4-D continuous frequency domain, which is given by the intersection of the two 3-D hyperplanes[29].

$$\Omega_x - m\Omega_u = 0 \quad (2.10a)$$

$$\Omega_y - m\Omega_v = 0 \quad (2.10b)$$

From the equation below, it is easy to see that the parameter α corresponds to the depth.

$$\tan \alpha = \frac{1}{m} = \frac{z_0}{D} \quad (2.11)$$

Where D is fixed and the depth z_0 is changeable. Thus, the ROS depends only on the depth z_0 of a Lambertian point source.

In the case of a Lambertian object, where the depth varies in a range, i.e. $z_0 \in [d_{min}, d_{max}]$, by using the linearity of the multidimensional Fourier transform[34], the ROS of the spectrum[29] can be obtained as

$$\mathcal{O}_{4C} = \bigcup_{z_0}^{[d_{min}, d_{max}]} \mathcal{P}_{4C} = \bigcup_{z_0}^{[d_{min}, d_{max}]} (\mathcal{H}_{4C,xu} \cap \mathcal{H}_{4C,yv}), \quad (2.12)$$

z_0 stands for a certain depth and the unification of all the depths is denoted by \mathcal{O}_{4C} which is the spectrum ROS of the object. Figure 2.14 illustrates the ROS \mathcal{O}_{4C} .

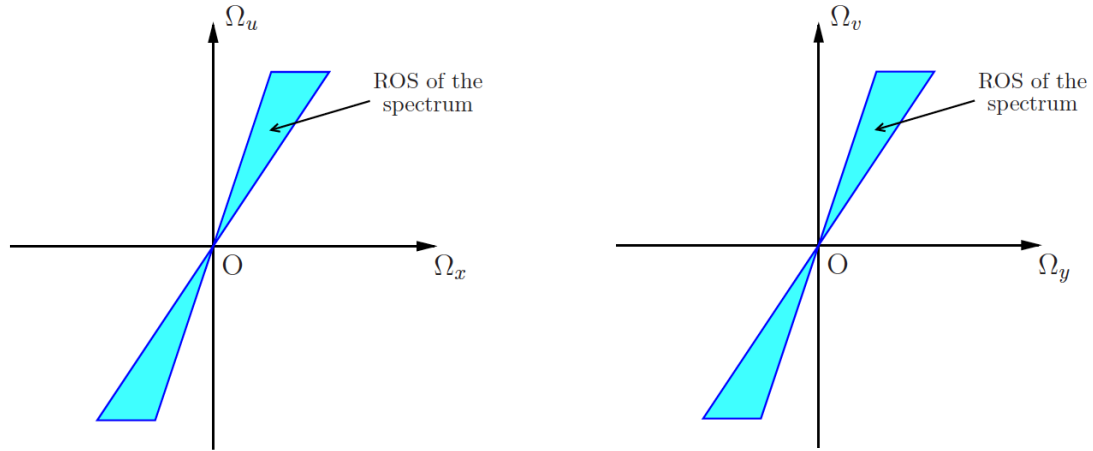


Figure 2.14 ROS of the Spectrum of a Lambertian Point Source 2[29]

2.4 Connection between LFs and Bokeh

As figure 2.13 and 2.14 shows above, the slope $\frac{1}{m}$ corresponds to the extent of how far the light source to the camera plane is. The slope is denoted as α in the following chapters. When changing the α , the depth of focus is moved from back to front or from front to back of the image. The blue region in figure 2.14 is the ROS of the signal in frequency domain which corresponds to the DOF in an image. Signals in this region corresponds to the part of the image which appear sharp and those outside the blue region would be blurred which we call it bokeh.

This project is based on the connection of LF depth and bokeh. In the next section, LF data will be used for volumetric refocusing. The depth will be adjusted by applying hyperfan filters we will find the best parameters which can present a pleasant visual effect of bokeh.

2.5 Summary

This chapter introduces some fundamental knowledge about geometrical optics, details of LF and representation of LFs in 4-D frequency domain as well as the connection between LFs and bokeh in frequency domain. Next chapter would illustrate the design of 4-D hyperfan filter that based on the knowledge of this chapter.

Chapter3 Comparison and Analysis

This chapter discusses the design of a proposed 4-D FIR hyperfan filter for refocusing and the evaluation of the performance of the fan filter for various design parameters. Comparisons and analysis are made using different LFs and different parameters. Based on these comparisons, conclusions are drawn about the effect of fan filters on the quality of the refocused images.

3.1 Proposed 4-D FIR Hyperfan Filter

2-D FIR fan filter is designed and created based on the second method (rotated fan filter) presented in [32,33]. The FIR is obtained by employing a 2-D window function. The objective of applying different filters to the same LF data is to analyze what kind of fan filters can provide relatively better visual effects of bokeh. The spectral ROS of a Lambertian object and the passband of the 4-D hyperfan filter $H(\mathbf{z})$ in the $\omega_x\omega_u$ subspace is shown in figure 3.1.

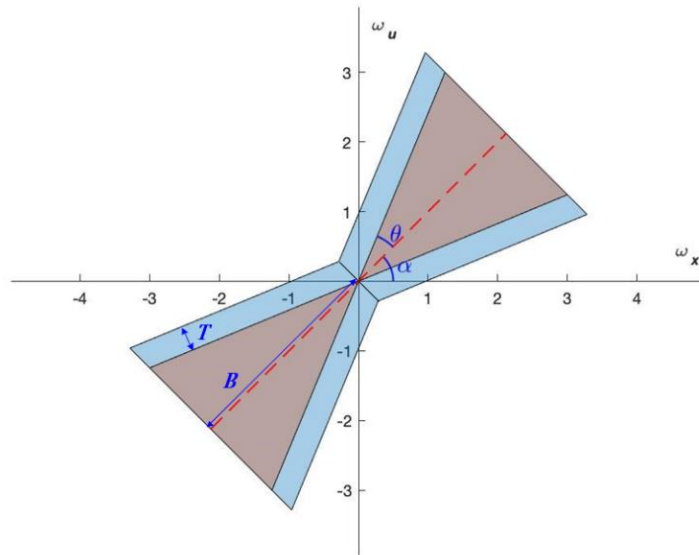


Figure 3.1 The spectral ROS of a Lambertian object and the passband of the 4-D hyperfan filter $H(\mathbf{z})$ in the $\omega_x\omega_u$ subspace

B is the bandwidth of the filter and is set equal to 0.9π (i.e. 0.9 of the Nyquist frequency). T is the width of the secondary passband which is set equals to 0.08π . There are two parameters in the hyperfan filter that can be changed and result in different visual effects of bokeh, namely θ and α .

From the figure 3.1, θ and T determines the angular width and α determine the orientation of the bow-tie-shaped passbands. The order of a FIR filter is a number describing the highest exponent in the numerator of the z-domain transfer function of the filter. According to [33], the order of the 4-D hyperfan filter $H(\mathbf{z})$ is $M_x \times M_y \times M_u \times M_v$, where $H(\mathbf{z})$ is the impulse responses and $M_x, M_y, M_u, M_v \in \mathbb{N}$. By changing the opening (θ) and angle of rotation (α) which corresponds to a fixed depth, we can distinguish which one results in the best aesthetic effect of bokeh by visually inspection.

3.2 Design of 4-D FIR Hyperfan Filter

The proposed 4-D FIR hyperfan filter [33] $H(\mathbf{z})$ used for volumetric refocusing of LF, $(z_x, z_y, z_u, z_v) \in \mathbb{C}^4$, is designed as a cascade of two 4-D hyperfan filters, namely $H_{xu}(\mathbf{z})$ and $H_{yv}(\mathbf{z})$. Due to the partial separability of the spectral ROS \mathcal{O}_{4C} (see equation in section 2.3), the passbands of $H_{xu}(\mathbf{z})$ and $H_{yv}(\mathbf{z})$ are respectively applied to encompass the hyperfans given by $\mathcal{B}_{xu} = \cup_{z_0} \mathcal{H}_{4C,xu}$ and $\mathcal{B}_{yv} = \cup_{z_0} \mathcal{H}_{4C,yv}$ (see eq2.8 and eq2.9).

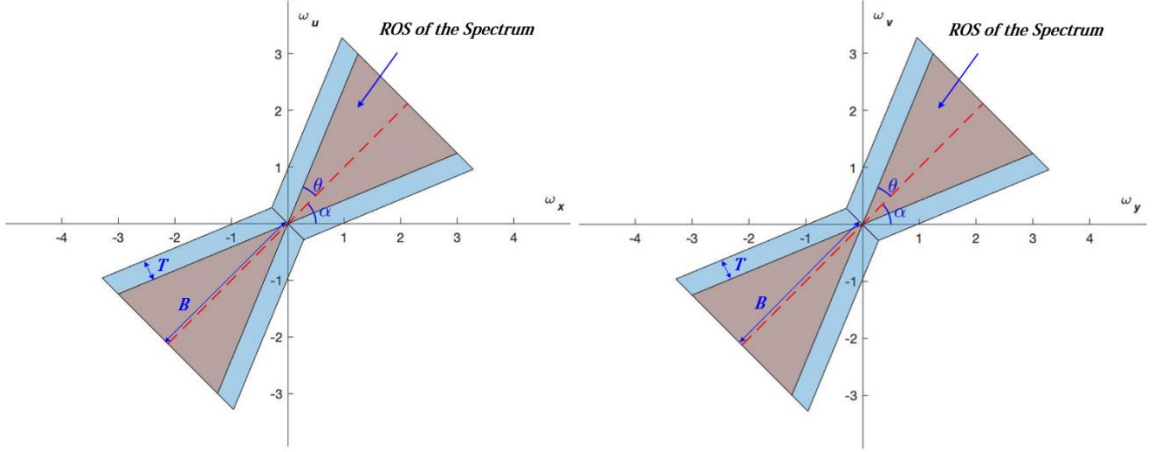


Figure 3.2 The ROS of the Spectrum and the passband of the 4-D hyperfan filter $H(\mathbf{z})$ in the $\omega_x \omega_u$ subspace and $\omega_y \omega_v$

3.2.1 Coefficients of $H_{xu}(\mathbf{z})$ and $H_{yv}(\mathbf{z})$

Due to the independency of ω_y and ω_v from \mathcal{B}_{xu} , as well as the independency of ω_y and ω_v from \mathcal{B}_{xu} , the 4-D FIR hyperfan filters are reduced to 2-D FIR fan filters. In this project, the 2-D FIR fan filter proposed in [32] is being used. This filter has a bow-tie-shaped passbands instead of a pure fan-shaped passbands because near the origin of the 2-D frequency domain are poorly approximated by 2-D FIR filters in $\omega_x \omega_u$ and the $\omega_y \omega_v$ subspace. Since a secondary passband is inserted between the main passband and the stopband, the low-frequency response has been improved.

According to [33], the order of the 4-D hyperfan filter $H(\mathbf{z})$ is $M_x \times M_y \times M_u \times M_v$, where $H(\mathbf{z})$ is the impulse responses and $M_x, M_y, M_u, M_v \in \mathbb{N}$. The coefficients, also called the impulse response of $H_{xu}(\mathbf{z})$ of order $M_x \times 0 \times M_u \times 0$, as well as $H_{yv}(\mathbf{z})$ of order $0 \times M_x \times 0 \times M_u$ are obtained as

$$h_{xu}(\mathbf{n}) = [h_{xu}^l(n_x, n_u)w_{xu}(n_x, n_u)\delta(n_y)\delta(n_v)] \quad (3.1a)$$

$$h_{yv}(\mathbf{n}) = [h_{yv}^l(n_y, n_v)w_{yv}(n_y, n_v)\delta(n_x)\delta(n_u)] \quad (3.1b)$$

where $h_{xu}(n_x, n_u)$ and $h_{yv}(n_y, n_v)$ are the ideal infinite-extent impulse responses (IIR), and $w_{xu}(n_x, n_u)$ and $w_{yv}(n_y, n_v)$ are 2-D separable windows.

3.2.2 Selection of the 2-D Window Functions

$w_{xu}(n_x, n_u)$ and $w_{yv}(n_y, n_v)$ are 2-D separable windows of size $(M_x + 1) \times (M_u + 1)$ and $(M_y + 1) \times (M_v + 1)$ [33]. In designing a 2-D FIR fan filters to attenuate interferences and noise, where higher stopband attenuations are required, the 2-D separable Hamming or Kaiser windows [34], [35] are frequently employed. However, in LF volumetric refocusing, we want to only blur stopband objects rather than completely attenuating them, and a rectangular window would be enough.

3.3 LF Dataset

A LF is fundamentally a 4-D structure. Each pixel corresponds to a ray, and two dimensions define that ray's position, while the other two are used to define its direction.

In this chapter, LF data "University" and "Magnet" are used and they are derived from "EPFL Light-Field Image Dataset" provided by MULTIMEDIA SIGNAL PROCESSING GROUP MMSPG at EPFL [31]. The file is in "MAT" format with five dimensions which can be directly used in MATLAB without further modification. LF data from EPFL are of size $15 \times 15 \times 434 \times 625 \times 4$. The last dimension is 4 with three RGB color channel and one weight channel. This four-channel format is convenient and helpful in processing LFs. The weight channel presents the confidence associated with each pixel. It's likely that the weight channel will be useful in filtering operations like ignoring zero-weight pixels in future applications of LFs which accept the weighting term. However, in this project, weight channel is not needed when doing refocus or visualizing LFs.

The center images of two original LFs are shown below.



Figure 3.3 Center Image of LF "University" (left) and "Magnet"(right)

In order to test the effect of each fan filter parameter, different size LFs are used in the experiment. A LF named "Dishes" originating from [8] and of size $9 \times 9 \times 512 \times 512 \times 3$ and another LF named "Ankylosaurus and Diplodocus" of size $15 \times 15 \times 434 \times 625 \times 4$ are used for this analysis.

Conventionally, the lenslet is indexed by the pair k, l (k is horizontal), and the pixel within the lenslet is indexed by i, j (i is horizontal). With Lytro's lenslets each one yields 9×9 useful pixels and the Lytro imagery yields approximately 512 pixels in both k and l , the decoded LF would be a 5-D array of size $9 \times 9 \times 512 \times 512 \times 3$. The indexing order for LF is j, i, l, k, c , where c is the RGB color channel.

The central image of LFs for verification are shown in figure 3.4.



Figure 3.4 Most Centered Image of LF “Dishes” (left) and “Ankylosaurus and Diplodocus”(right)

3.4 Effect of Alpha

The two parameters which are used in the design of different 4-D fan filters are α and θ . As shown in the previous section, α is associated with depth, while θ is associated with DOF. Here, we start by visualizing the effect of changing α and keeping θ constant.

Two experiments are conducted with $\theta = 30$ and $\theta = 1$ respectively. The central image of the LF after 4-D filtering is shown in figure 3.5 and figure 3.6.

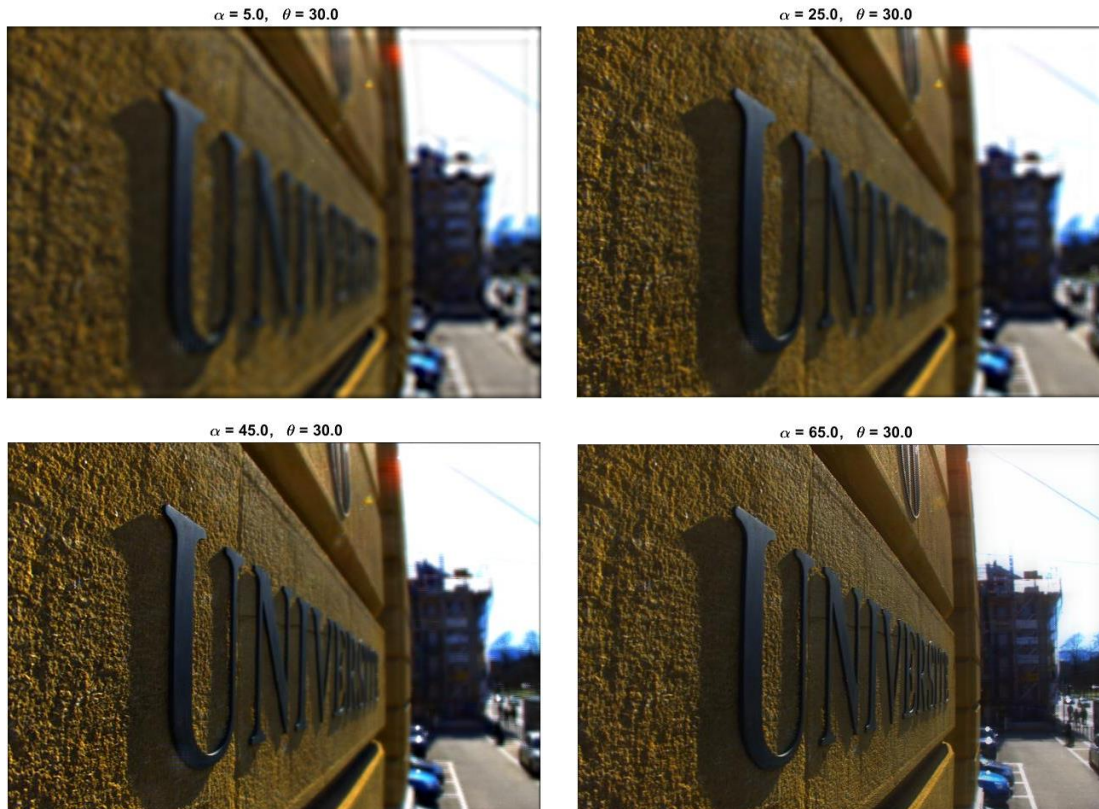




Figure 3.5 Refocused LF Image for Different α

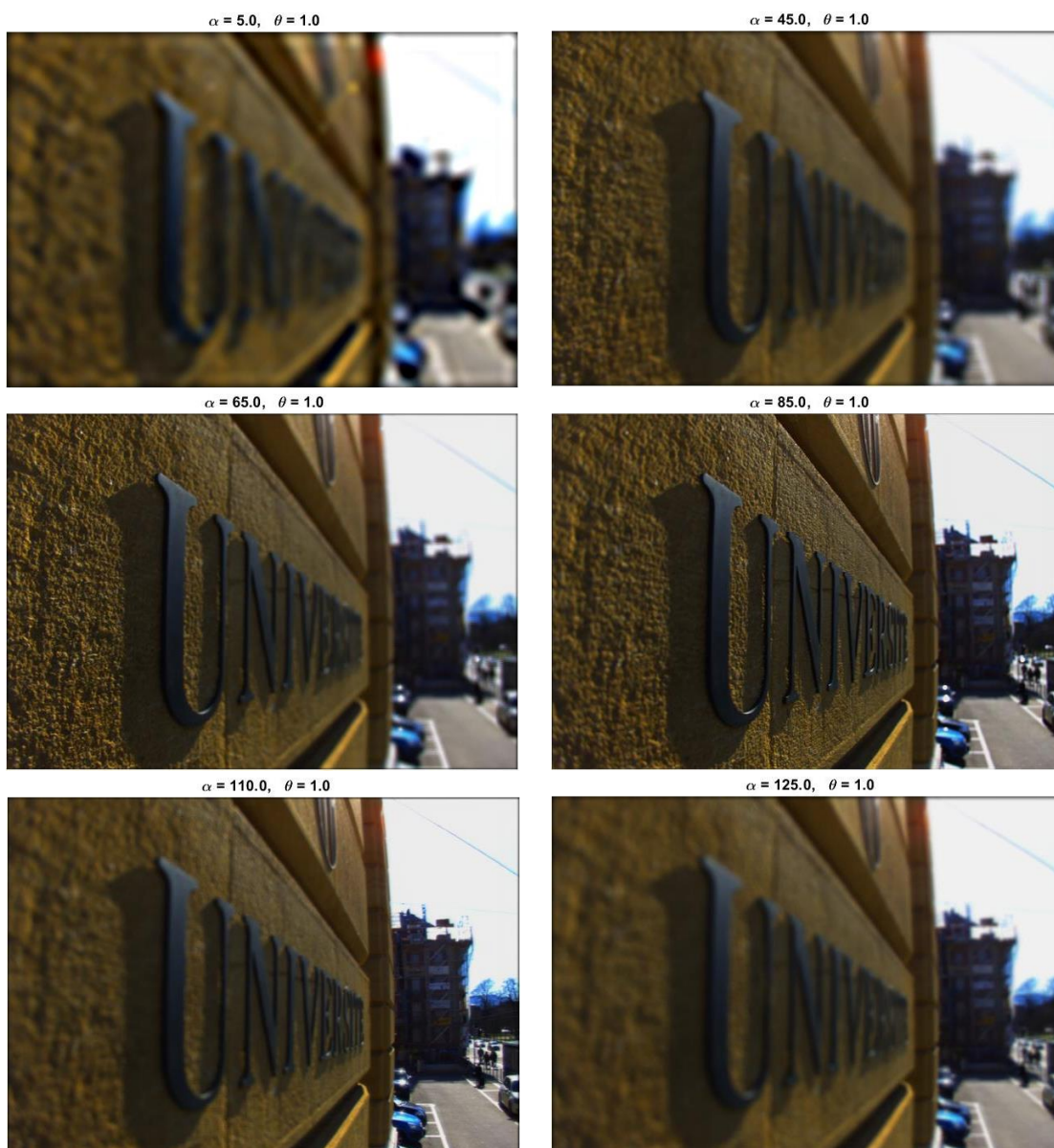


Figure 3.6 Refocused LF Image with Different α

The following is observed from the above images with $\theta = 1$. Increasing the α would move the focal plane from front to back. For example, parts of the image would appear in focus at different depths. When $\alpha = 10$, the sign “U” and objects behind it are totally blurred. When α increases to 50, we can see the sign “U” becomes sharp and objects behind it are still blurred but sharper than before. And as α increases to higher (65 – 85), we get a larger depth range in focus, so more parts of the image appear sharp. Continuously increasing α , the front of the image is getting blurred which means the focal plane is moving backwards.

Further, a pleasant bokeh can be observed for $\alpha = 65$. This can be explained that a small α would result in most part of the image blurred while larger α would result in little part of the image blurred. In these two occasions, main object of the image may be lost and there would be little chance to generate bokeh respectively.

Thus, according to the results, parameter α controls the distance between the focal plane and camera plane. When increasing α , we are moving the focal plane away from the camera, vice versa.

3.5 Effect of the angle θ (Opening) of Fan Filter

To figure out the effect of the opening of fan filter, α is set equal to 90. Because when α equals to 90, the focus of the image exactly falls on the object on the right of the image (magnet) which would help to understanding the effect of θ .

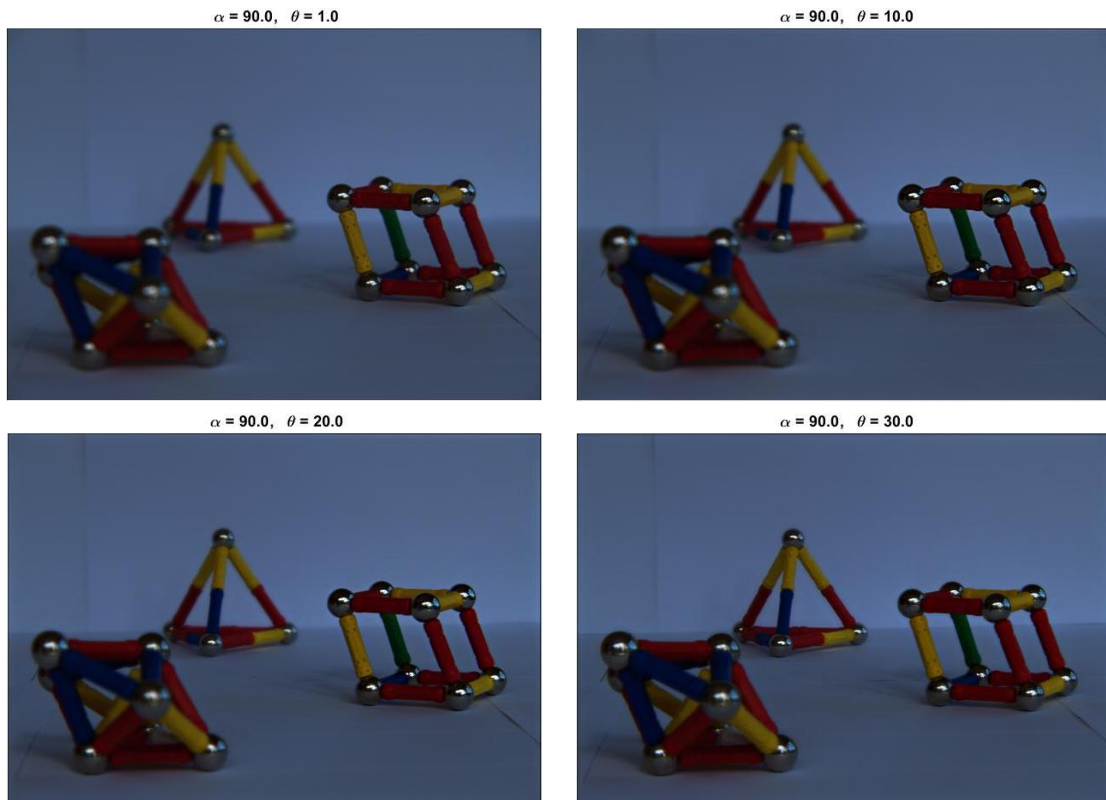


Figure 3.7 Refocused LF Image with Different θ

From the images in figure 3.7, it can be seen that when $\theta = 1$, the object on the left (magnets) at the back and front are at an out-of-focus position while the right magnet is right in focus. By comparing the cases $\theta = 1$ and $\theta = 20$, it can be seen that when $\theta = 1$, magnets at the front and back are more blurred than the case when $\theta = 20$. As θ increases, the magnets at front and back are becoming increasingly sharp. At $\theta = 30$, several details can be easily distinguished. Thus, the object located in the depth range corresponding to the passband of the 4-D hyperfan filter appear sharp in the refocused image and with a small opening is likely to generate bokeh. The figure 3.8 shows the general view and top view of magnitude response of the corresponding hyperfan filter with $\theta = 10$.

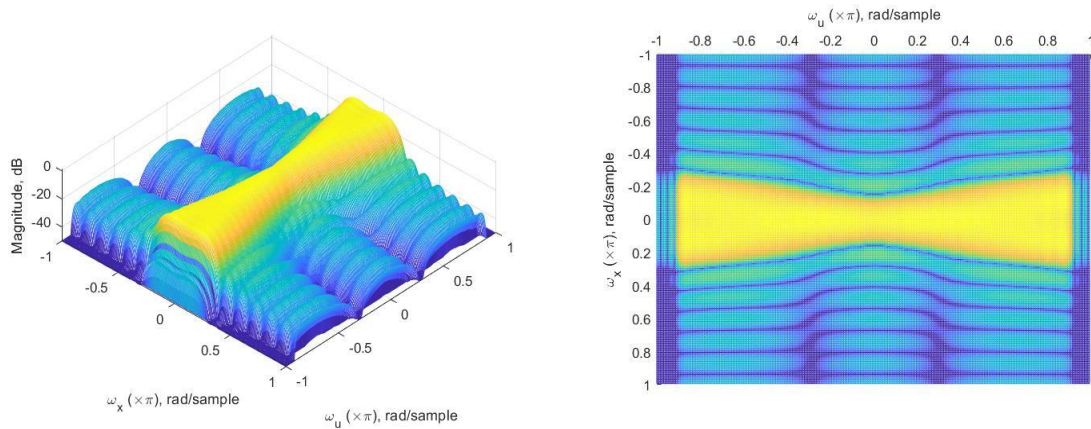


Figure 3.8 Magnitude Response of Hyperfan Filter with $\alpha = 90$ and $\theta = 10$

The magnitude response of the hyperfan filter in figure 3.8 displays a sharp passband colored in yellow and the stopband colored in blue where signals are attenuated and appear blurred. The signals in the area colored in yellow corresponds to the area where signals appear sharp in the refocused image while the signals in the blue area appear blurred. The objects having depths corresponding to the stopband of the 4-D hyperfan filter appear blurred. A small θ corresponds to a small range of DOF while larger θ corresponds to a greater range where less part of the image gets blurred.

In a word, the parameter θ controls the range of DOF. The larger the θ , greater the range of DOF, vice versa.

3.6 Additional Examples

According to section 3.4 and 3.5, we know that α and θ correspond to depth information and opening of the fan filter. In this section, we would show consistent results using LFs of different size.

3.6.1 LF Data of size $15 \times 15 \times 434 \times 625 \times 4$

The α is associated with depth and we can change the depth by changing the α . By changing the α , we would see different parts of the image are in focus each time.

An appropriate α is measured by fixing the θ , θ is set equal to 10 here.

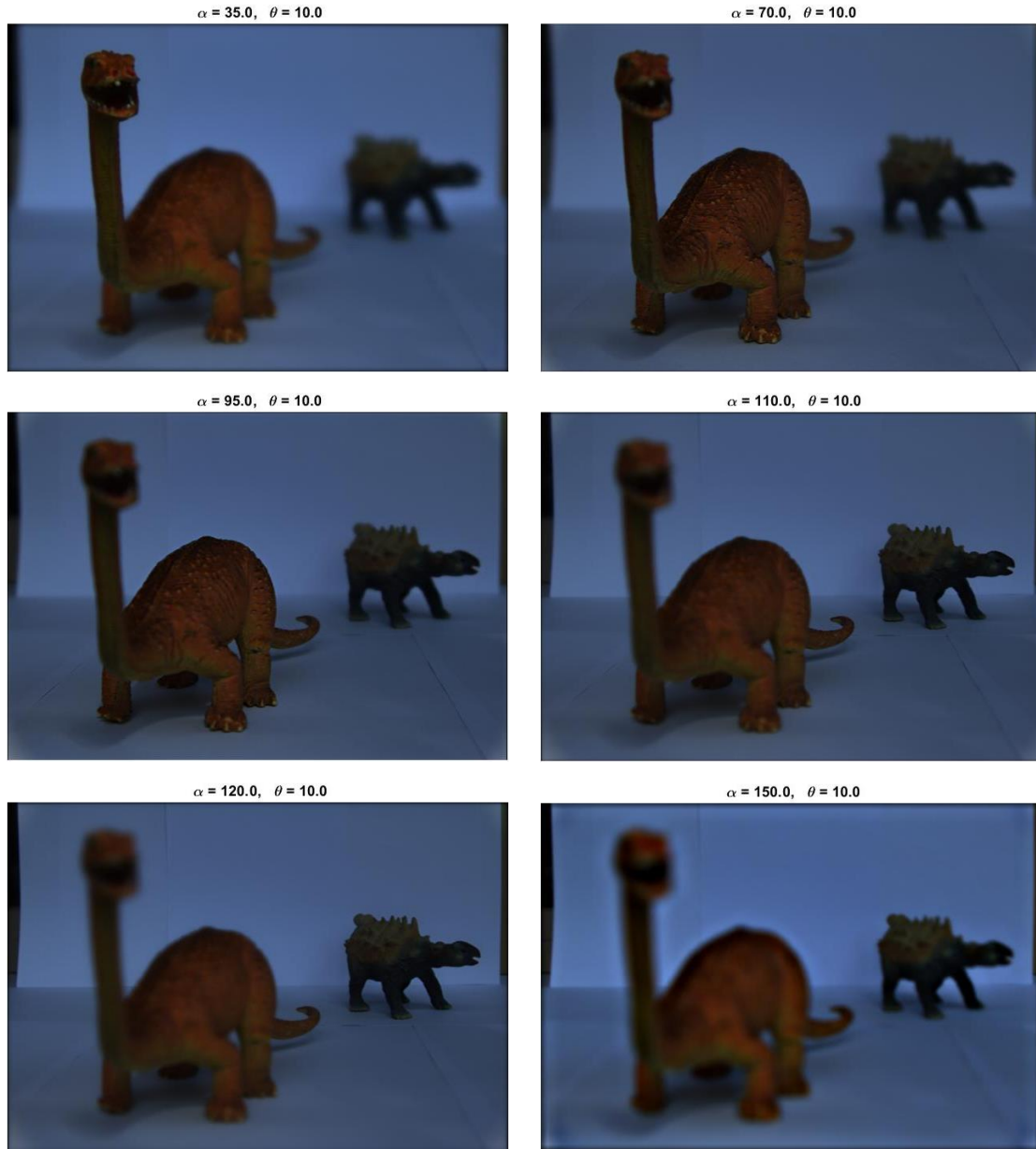


Figure 3.9 Refocused LF Image with Different α

When α equals to 35, through inspection, the focus is at the head of diplodocus at the front. When α increases to 70, the focus moves to the back of diplodocus (object on the left). Continuously increasing α , we can see the focus of the refocused image move to the ankylosaurus at the back while the diplodocus is totally blurred.

In the case where the head of diplodocus is the subject of interest of the image, it would be good to have $\alpha = 35$. By choosing $\alpha = 35$, an image with focus on the head of diplodocus gives us a desired DOF which will get an acceptable bokeh. If one wants to highlight different part of the image, other value of α would be appropriate.

Thus, α is set equal to 35 here. Then, we can adjust the DOF by changing θ .

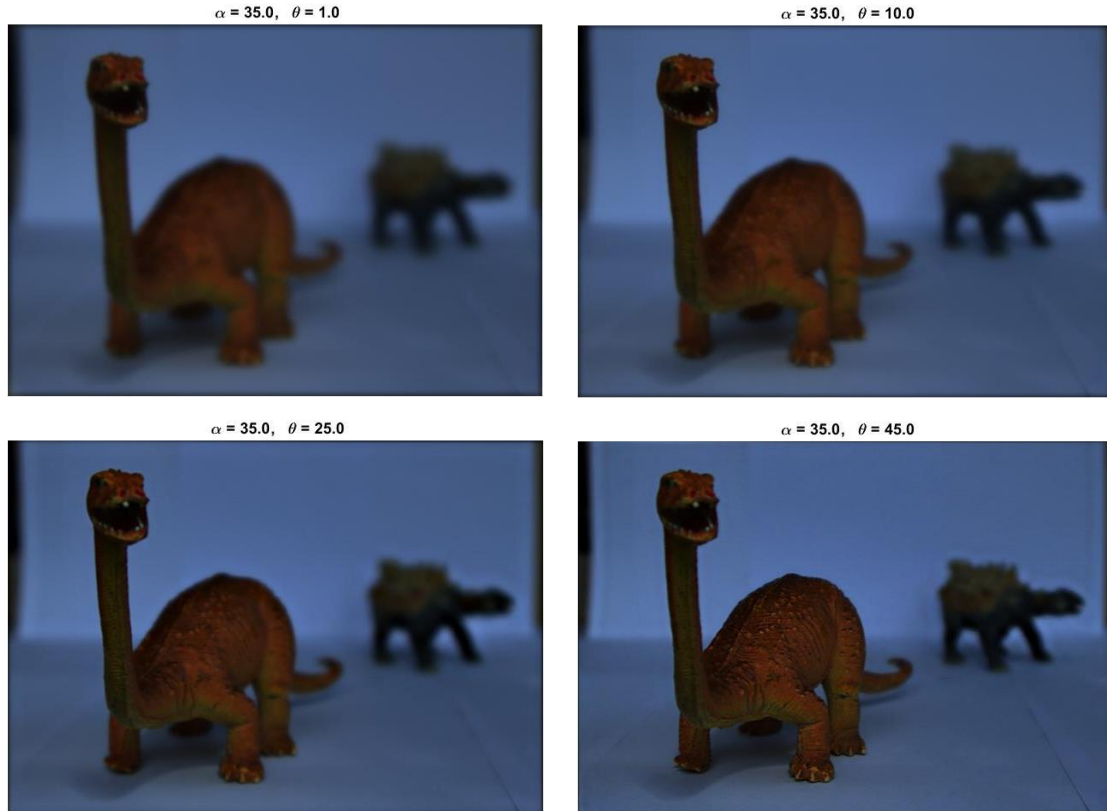


Figure 3.10 Refocused LF Image with Different θ

When θ equals to 1, through inspection, the focus is at the head of diplodocus at the front. Except the head of diplodocus is in focus, other part of the image is blurred because the extremely small θ . Due to $\theta = 1$, range for DOF is small. As θ increases, we can see the range for object in focus is extended.

3.6.2 LF Data of size $9 \times 9 \times 512 \times 512 \times 3$

A LF of different size is evaluated in this section.

Due to the subject of interest of this LF is the objects (dishes and a bird) in the box, so the α that makes the focus located inside the basket would be an appropriate one to analyze the effect of two filter parameters.

Therefore, an appropriate α is measured by fixing the θ to a constant, θ is set equal to 15 here.

To note that θ can be other values here, but a smaller θ will help distinguish the position of focus better than the greater one.



Figure 3.11 Refocused LF Image for Different α

α ranging from 10 to 150 are tried and the most typical results are shown above. It is evident that when $\alpha = 10$, the front of the image is sharp, and we can only see the table clearly while other parts are blurred heavily. As α increases to 40, the table, first dish and the front of the case appear sharp. Because the focus of the image is moving from front to the back of the image. It can be easily found that when $\alpha = 130$, the focus moves away to somewhere between the last dish and the bottles.

As expected, the α controls the distance from focal plane to camera plane. The focus moves away when α increases and moves to the front when α decreases.

In the case where objects inside the basket are the subjects of interest of the image, it would be good to have $\alpha = 75$. By choosing $\alpha = 75$, an image with focus located inside the basket gives us a desired DOF which will get an acceptable bokeh. Similarly, to evaluate the best value of θ , α is fixed equal to 75.



Figure 3.12 Refocused LF Image for Different θ

When $\theta = 5$, evident transitions from blurred to sharp can be seen at the front and back of the image respectively. And the first two dishes are sharp while the latter two are blurred. When θ increases from 5 to 50, four dishes become sharp.

With a fixed α , the focus remains the same point all the time in the four images above. Thus, it can be concluded that the range of DOF increases as θ increases. So, the reason for there are more area staying in focus is that the increase of DOF.

3.7 Discussion

What the experiments show is that we can choose α and θ to obtain satisfactory bokeh and this can be done by post-capture refocusing. We can choose an α by deciding what part of the image will be in focus. Then, we can choose a DOF by changing θ . In this way, we can get an acceptable DOF and a visually pleasant bokeh.

3.8 Summary

In this chapter, the design of 4-D hyperfan filter is outlined and its frequency response characteristics in the 4-D frequency domain are illustrated. It is shown that the center line of the fan is related to the distance of the object from the image plane and the opening angle of the fan is related to the DOF. Various LFs were processed using different values of α and θ to visually demonstrate, refocusing at different depth, changing DOF and generating bokeh.

In the next chapter, a software tool will be introduced which can be used to do post capture refocusing interactively.

Chapter4 Software Design

The objective of this project is designing a tool for refocusing of LFs. In this chapter, work of designing and implementing a graphical user interface (GUI) for design filtering and presentation of LFs is presented. In this project, the toolbox from Donald G. Dansereau [37] is used to display LFs and software developed by Chamira Edussooriya et al in [33] and [2] is used to do refocusing. The structure of the software tool and how each function works, as well as how to use the tool by providing detailed instructions.

4.1 Specification and Structure

This software is implemented in MATLAB with MATLAB version 2018b and it is deployed on Windows 10. The motivation for the design of this system is to help those who are not familiar with the LF to have a better understanding of the volumetric refocusing by providing an appropriate GUI to do analysis as the one presented in the previous sections.

The tool has mainly three functions, namely, display LFs as a video, extract central image of a LF and refocusing of LF. The functional block diagram for my software tool is shown below.

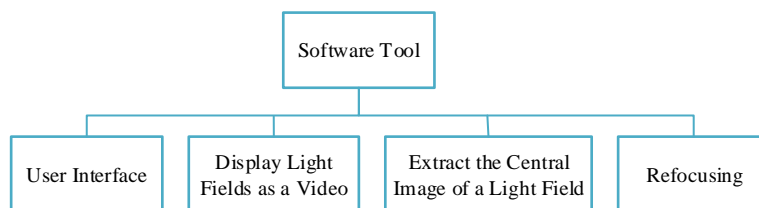


Figure 4.1 Software Tool Functional Block Diagram

4.2 Interface Design

The functional block diagram of the user interface module is shown below.

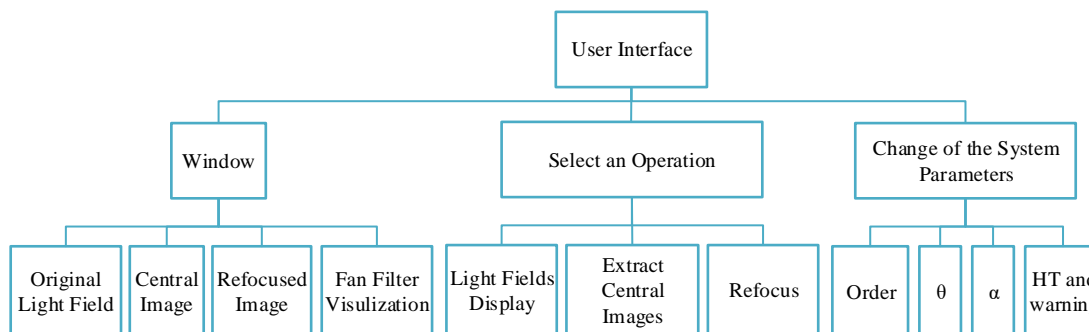


Figure 4.2 Functional Block Diagram of GUI Module

The following section introduces how the layout and basic functions of the software are designed. MATLAB provides a simple tool for the design of a GUI by just typing 'guide' in the MATLAB command line as shown below.

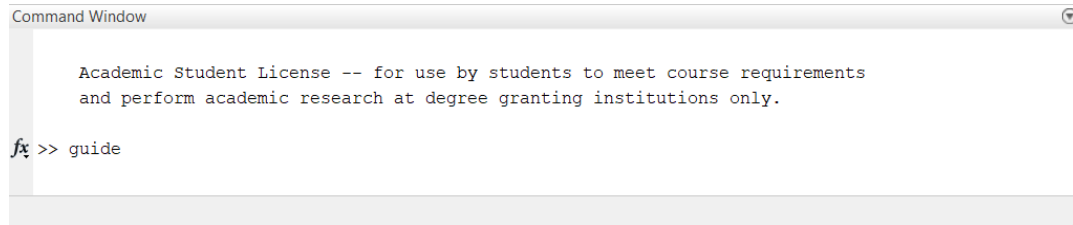


Figure 4.3 Start to Design a Layout for GUI

In the rest of the section, the use of MATLAB “guide” function to obtain the GUI is described.

Press the “enter” button and we will see a file selector in the middle of the MATLAB workstation. A new GUI can be created, or an existed GUI can be opened. Here, the file named “test.fig” which is the GUI file of this program is chosen and then press “open”.

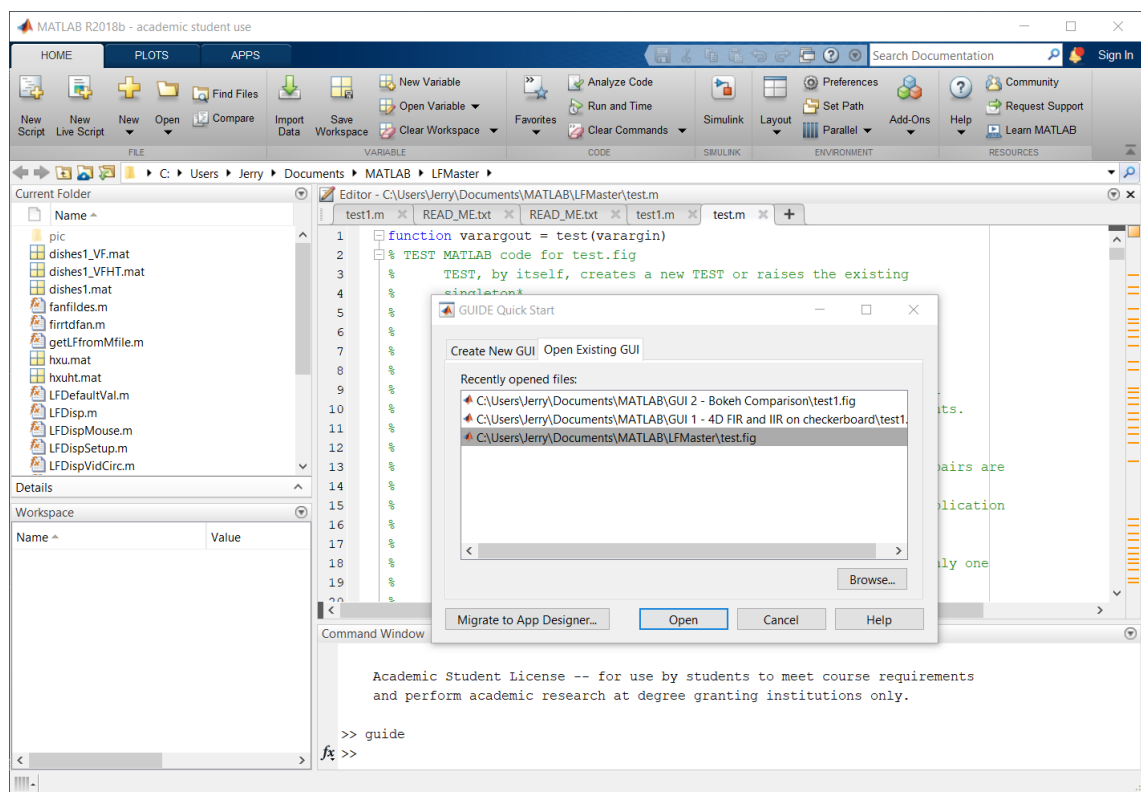


Figure 4.4 Screenshot of Opening GUI Guide

Now the following screenshot show where the interface of this program is designed. There are many kinds of tools, for example: push button, slider, check box, axes, pop-up menu and so on. By dragging the component needed from the left side to the right side, the interface could be simply created. Automatically, the system will generate a callback function where the code is written.

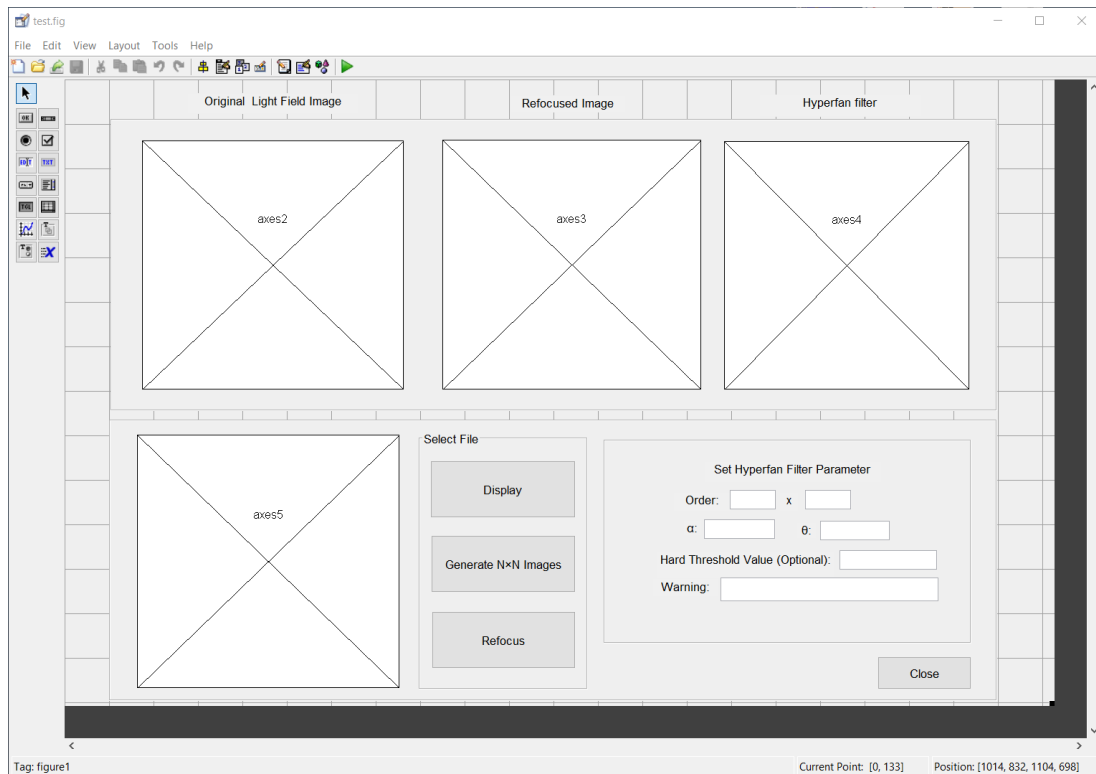


Figure 4.5 Screenshot of GUI Design

Press the “run” button, the program starts to run, and you will see the following interface.

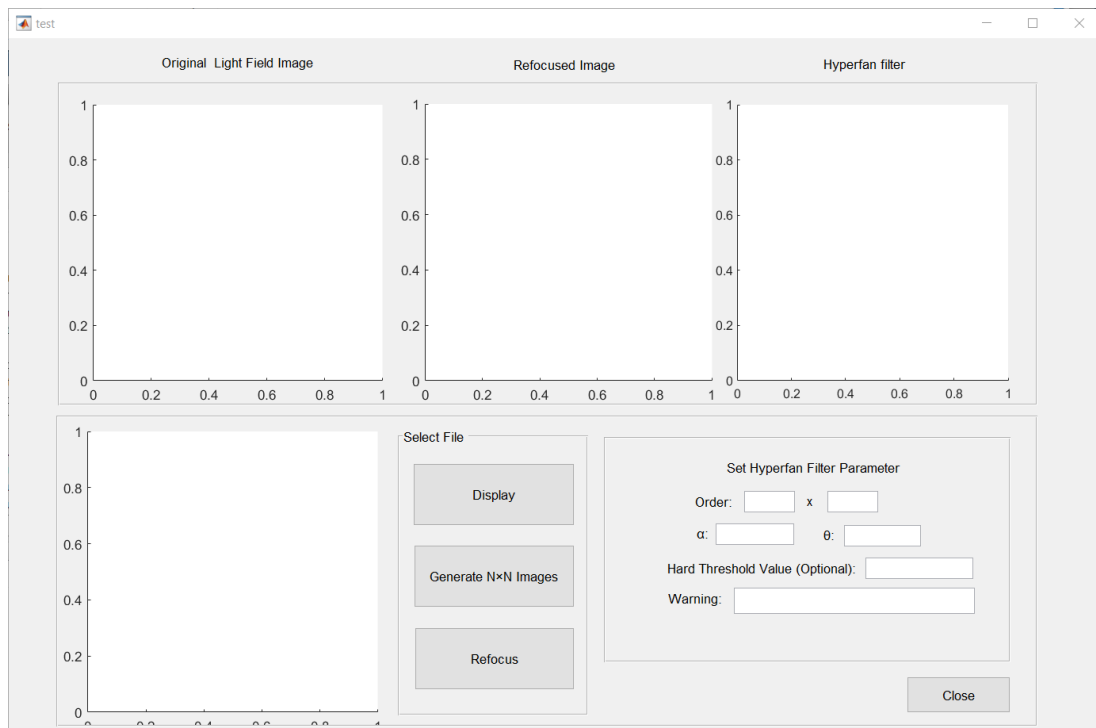


Figure 4.6 Screenshot of GUI

The interface designed using the approach described lead to a GUI shown in the screenshot of figure 4.6. It is divided into two parts, six components in total. The upper part is made up of three planes, displaying the center image of original LF, refocused image and the filter applied in refocusing respectively. The other part consists of one image plane, one function panel and one part to set the parameters for the filter. The image plane at the lower left corner displays a short video of original light field which is different from the first part. The function panel consists of three buttons, namely “Display”, “Generate $N \times N$ Images” and “Refocus”. Those are the functions that will be introduced at the following part. The lower right corner is a place where a user can enter manually the parameters for the fan filter.

The size of the whole interface is changeable and self-adaptive. By moving the mouse to any one of the boundaries and dragging the boundary, you can change the size of it. Automatically, the size of each component will also change to fit the whole interface.

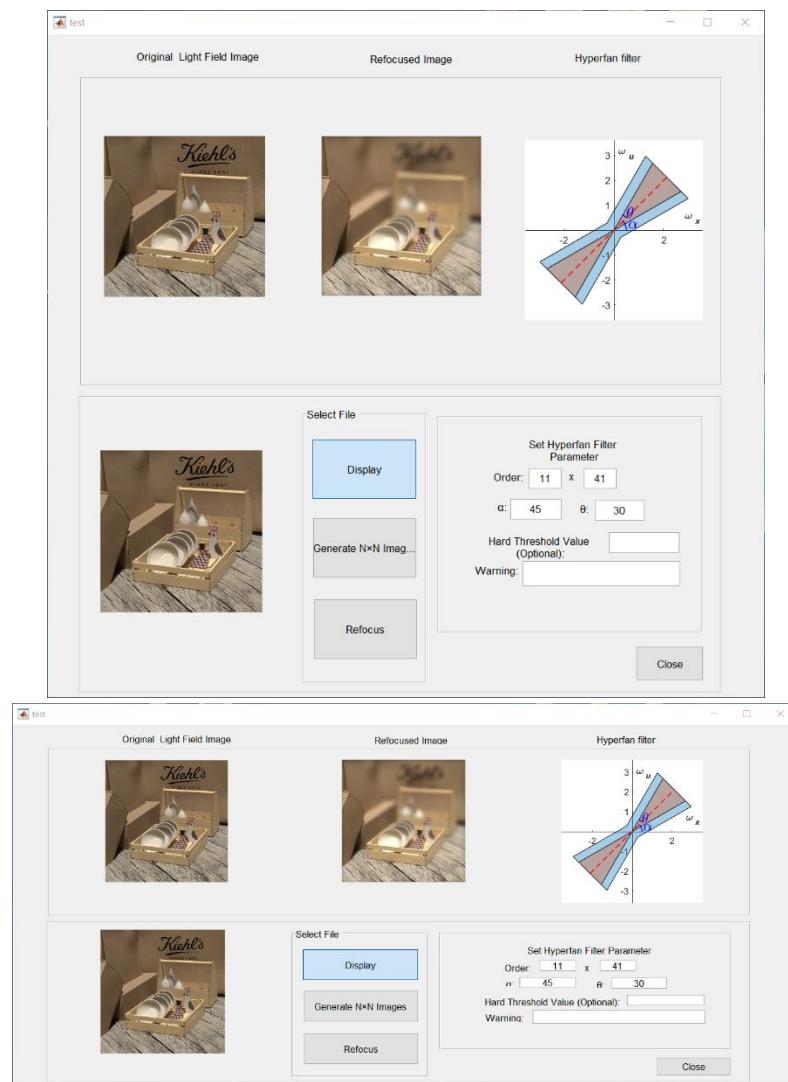


Figure 4.7 Screenshot of Size-adaptable GUI

4.3 LF Display as a Video

The objective is to download a LF and display it in the window as a video. The flow diagram of LF display module is shown below.

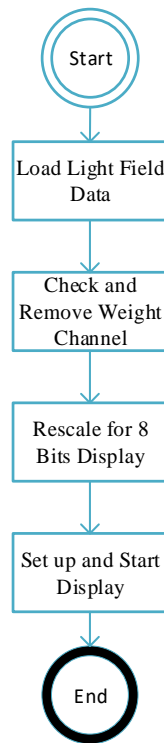


Figure 4.8 Flow Diagram of LF Display Module

After choosing the LF data, dimension of the data would be checked first. Due to the different source of LF dataset, the dimension may vary. The input may be a color or single-channel LF and can be float or integer format.

Then, to display the LF as a video, the LF array is converted to 8 bits per channel and if the LF contains more than three color channels, only the first three are used.

Finally, the light field is vividly displayed in the window where users would see the figure moving around just like a short video.

The LF used here is called ‘Dishes’, pictured as a 9×9 array of $512 \times 512 \times 3$ images, with the last dimension indexing color information.

Here is how to use the display function.

Presses the “Display” button and choose the file named “Dishes” in the file selector.

The following screen shows the display of a LF named “Dishes”. A short video consists of images from different views would be displayed in the lower left corner. It provides a very clear and straightforward method for users to see what the LF is.

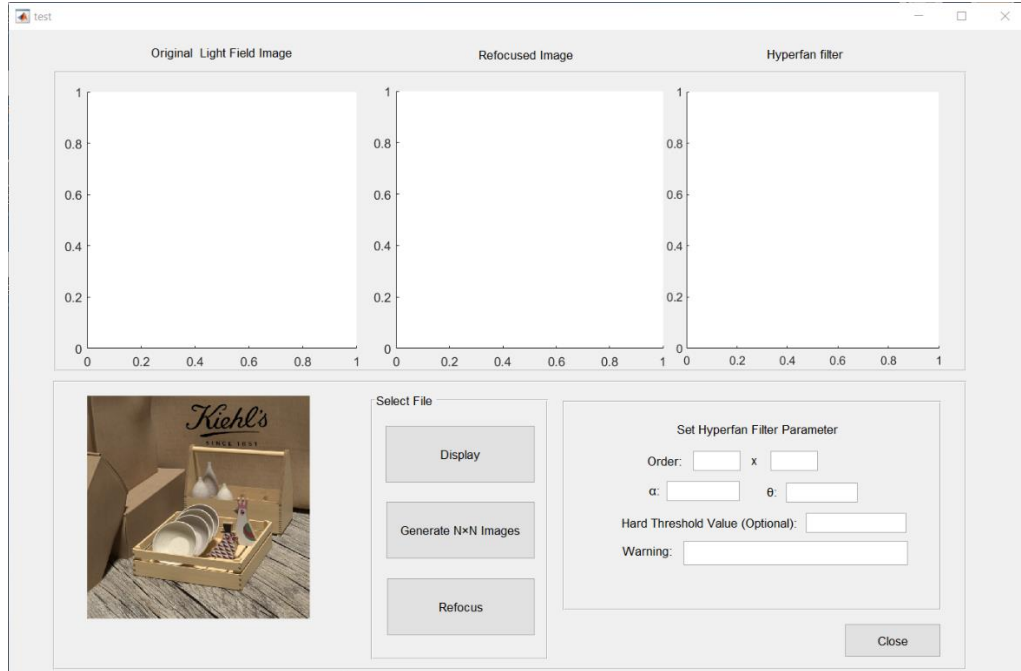


Figure 4.9 LF Display

4.4 Extract and Store the LF Images

The objective is to extract the $N \times N$ LF images from 4-D LF array and store the images in a specific file folder. The center image is included in these extracted images. The flow diagram of extract and store the LF images module is shown below.

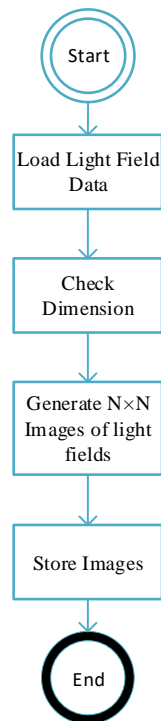


Figure 4.10 Flow Diagram of Extract and Store of LF Images Module

By clicking the “Generate $N \times N$ Images” button and choosing the LF you want to refocus, the software tool would automatically generate all the LF images and store them in a file folder name pic. The center image with the index $(\frac{N+1}{2}, \frac{N+1}{2})$ is also stored in the same folder.

The following screenshot shows the LF images for LF data “Dishes” in folder “pic”.

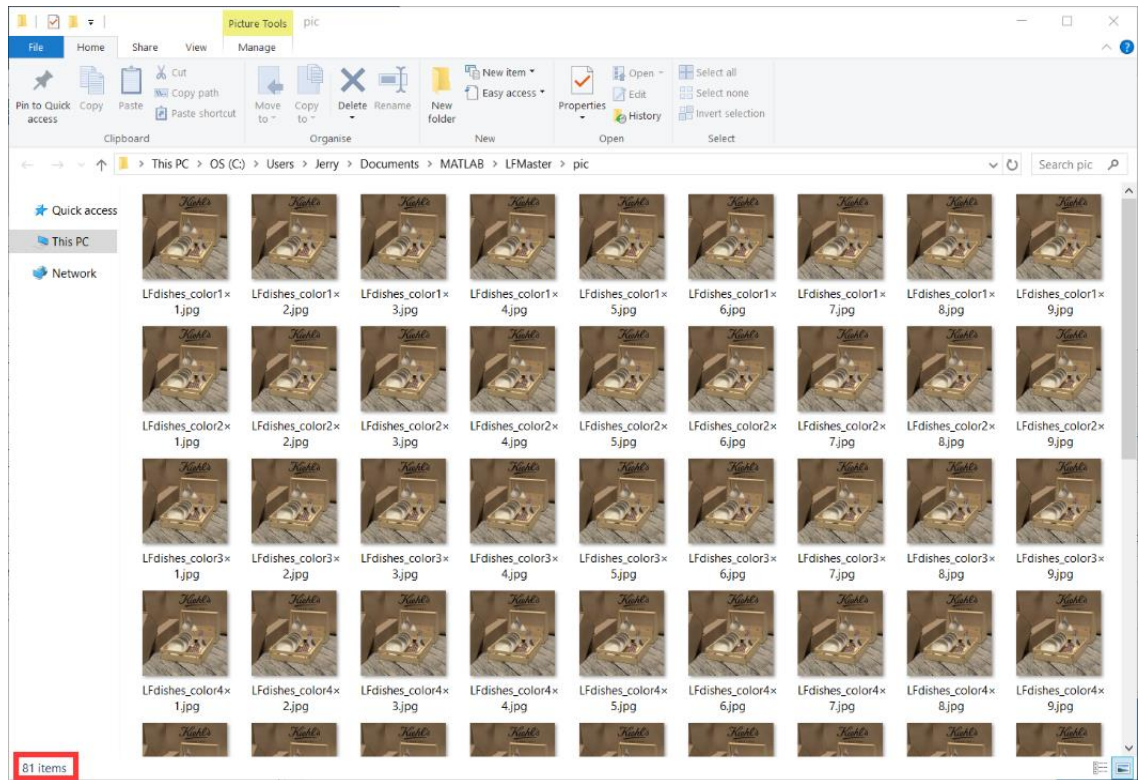


Figure 4.11 Screenshot of $N \times N$ Images of LF

The main purpose of this function is extracting $N \times N$ images of the LF. After loading the LF data, dimension of the data would be checked first as well. The implementation of this function relies on LF display function. It extracts the $N \times N$ images from the original LF data and stores each image at a time to the specific folder. N is the first and second length of dimension of the light filed, respectively. The LF used here is ‘Dishes’, a data of $9 \times 9 \times 512 \times 512 \times 3$. Thus, the N here is equal to 9. So theoretically, 81 images of this LF data would be generated. We can easily notice the lower left corner shows “81 items” which is exactly as expected.

The name of each extracted image is named as “Data Name + $N \times N$.jpg”, it is very convenient for the user to find for the image located at a specific position.

4.5 Volumetric Refocusing

The objective is that given a LF, fan filter parameters and order of the filter, the refocused image is generated and displayed in one of the windows. The flow diagram of volumetric refocusing module is shown below.

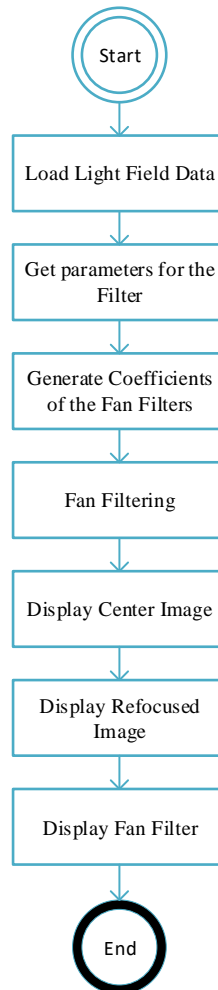


Figure 4.12 Flow Diagram of Volumetric Refocusing Module

When user finishes typing all the parameters needed for the filter, then press the “Refocus” button. You can see a file selector which is much convenient than typing an absolute path to select a file.

After successfully loading data, the parameters user typed in is passed to the function named “fanfiles” which is used to design the 2-D FIR fan filters required for volumetric refocusing. Hard thresholding is employed to reduce the computational complexity of fan filter. Here it is optional for user to set the threshold or not. The impulse responses are generated and saved as “hxu”. Then, the function named “volrefocus” is called. It implements the 4-D hyperfan filters for volumetric refocusing of the LFs.

The fan filters “hxu”, “hxuth” and light LF are loaded from directory and converted to frequency domain using function fast Fourier transform (FFT). Filtering is done in 4-D frequency domain to produce outputs “lfvf” with conventional depth filter and “lfvfh” with hard threshold depth filter (sparse filter). Output images are saved in “.mat” format.

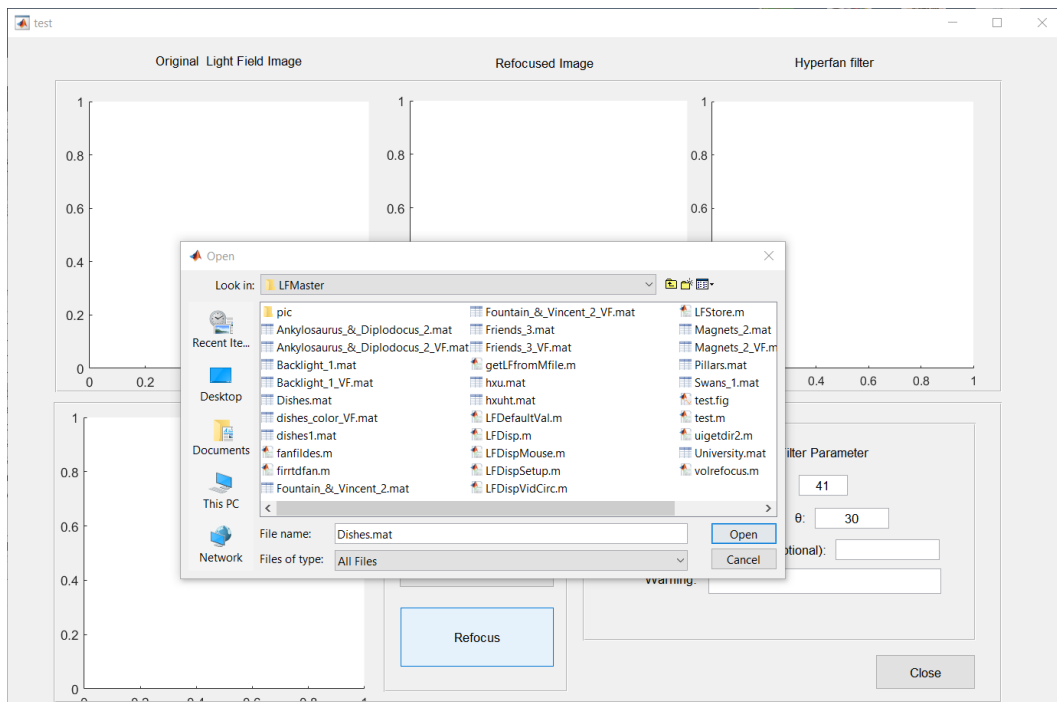


Figure 4.13 File Selector

After choosing a LF file, it would take a while for the computer to do the calculation and display the results. The following screenshot shows the original LF image and the image after refocusing. The layout here helps user easily see the difference of these two images. It also displays the filter which is applied to do the refocusing. It makes the whole process not abstract anymore because of these tools of visualization.

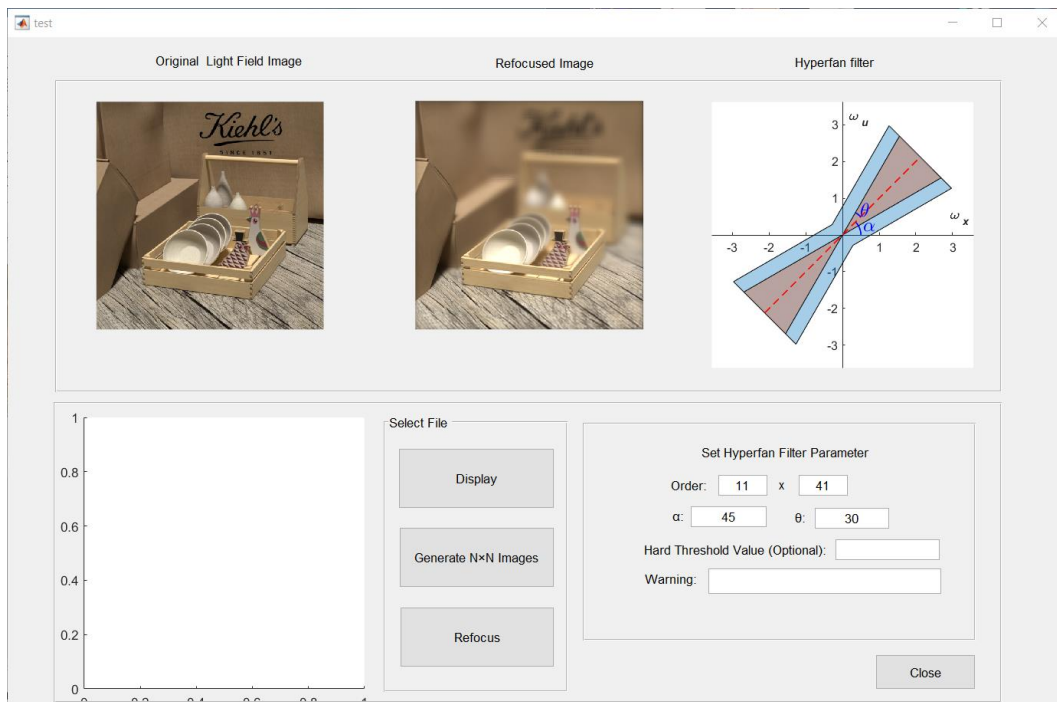


Figure 4.14 Refocusing of LF

All the function can work in a parallel way and the following screenshot shows all the functions run simultaneously.

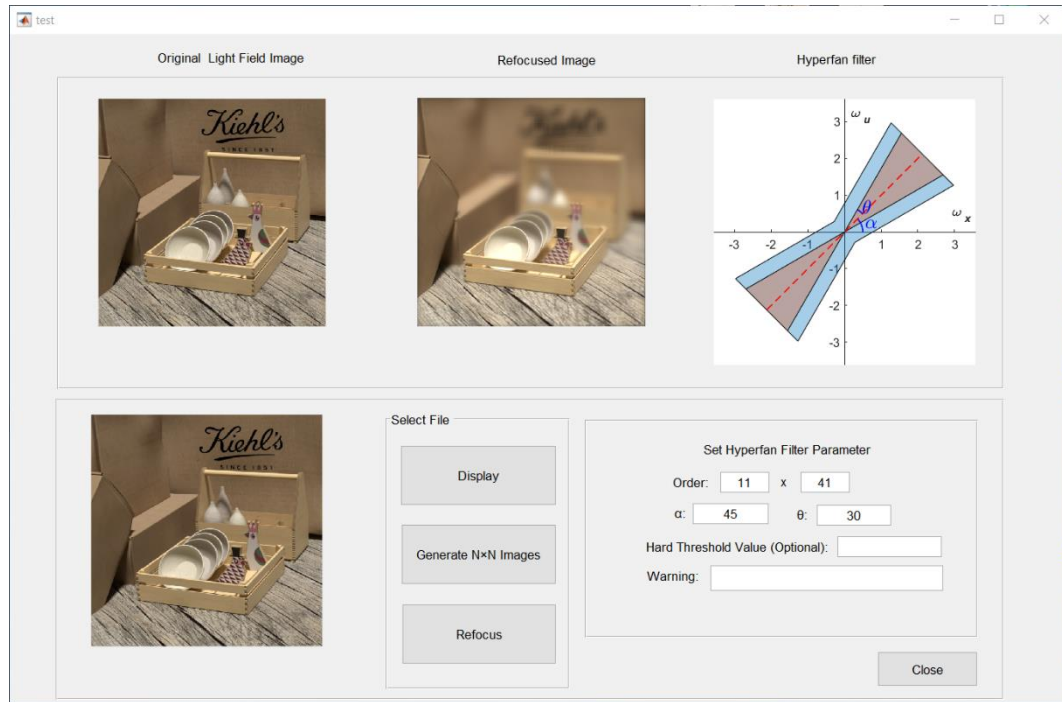


Figure 4.15 Screenshot of Fully Running Program

4.6 Summary

This chapter provides a detailed design of the GUI for refocusing of LFs. The structure of the whole software and each function is explicitly illustrated. Screenshots are presented to help understand how to use the tool.

Chapter5 Conclusions and Future Work

5.1 Conclusions

In this project, an interactive software tool is designed for volumetric refocusing of a light LF by using a post-capture refocusing technique. This software tool aims to help people like traditional photographers who do not know LFs to understand what the refocus of LF is and how the bokeh is generated.

Basic concepts of geometrical optics and bokeh are introduced for a better understanding of the analysis of a Lambertian object in frequency domain. The spectral ROS of a Lambertian point at a constant depth is analyzed [33] and shown to be two hyperfans in 4-D frequency domain. Based on the spectral analysis, a 4-D FIR hyperfan filter is designed for refocusing of the LF.

Furthermore, the design of 4-D hyperfan filter is outlined and its frequency response characteristics in the 4-D frequency domain are illustrated. It is shown that the center line of the fan is related to the distance of the object from the image plane and the opening angle of the fan is related to the DOF. Various LFs are processed using different values of α and θ to visually demonstrate, refocusing at different depth, changing DOF and generating bokeh. Experiments are conducted to evaluate the effect of these two parameters by using LFs of different size. Comparisons and analyses are made using different LFs and different parameters. Based on these comparisons, conclusions are drawn about the effect of fan filters on the quality of the refocused images. Experimental results confirm that filter parameter α controls the depth of the focal plane and θ controls the DOF of the refocused image.

The structure of the software and the design of each function is described. The software can be used to display a LF as a video, display the center image of the LF, display the refocused image and the figure of the filter used as well as to extract central images of the LF. The interactive user interface makes the refocusing of LFs easier. Screenshots were made as a guidance of how to use the software tool.

5.2 Future Work

Currently, there is not a general standard to measure whether a bokeh is good or bad, for comparisons made in chapter 3, the decisions are made visually and mostly depends on the observer's experience and personal aesthetic preference. Thus, when different users are using this software, they may have different opinions about whether it is a good or bad bokeh.

Future work can be done by exploring a general method for evaluating the quality of bokeh based on objective measure instead of subjective evaluations. Furthermore, the interactivity of the software tool is expected to be improved by providing more useful functions.

Reference

- [1] I. Ihrke, J. Restrepo and L. Mignard-Debise, "Principles of Light Field Imaging: Briefly revisiting 25 years of research," in *IEEE Signal Processing Magazine*, vol. 33, no. 5, pp. 59-69, Sept. 2016. doi: 10.1109/MSP.2016.2582220
- [2] Chamira Udaya Shantha Edussooriya, "Low-Complexity Multi-Dimensional Filters for Plenoptic Signal Processing", University of Victoria, 2015.
- [3] Thanh-Trung Ngo, Hajime Nagahara, Ko Nishino, Rin-ichiro Taniguchi, Yasushi Yagi, "Reflectance and Shape Estimation with a Light Field Camera Under Natural Illumination", *International Journal of Computer Vision* (2019) 127:1707-1722.
- [4] Ioana Speranta Sevcenco, "Multi-dimensional digital signal integration with applications in image, video and light field processing", University of Victoria, 2018.
- [5] Marcus Magnor, Bernd Girod, "Data Compression for Light-Field Rendering", *IEEE Transactions on Circuits and Systems for Video Technology*, vol. 10, NO.3, April 2000, 338-343.
- [6] Levoy, Marc, "Light field rendering." *Conference on Computer Graphics and Interactive Techniques ACM*, 1996:31-42.
- [7] "Lytro Company Fact Sheet". Lytro. Retrieved 24 June 2011.
- [8] Honauer K., Johannsen O., Kondermann D., Goldluecke B. (2017) A Dataset and Evaluation Methodology for Depth Estimation on 4D Light Fields. In: Lai SH., Lepetit V., Nishino K., Sato Y. (eds) *Computer Vision – ACCV 2016*. ACCV 2016. *Lecture Notes in Computer Science*, vol 10113. Springer, Cham.
- [9] "The Ultimate Guide to Learning Photography: Bokeh Background", <https://www.creativelive.com/photography-guides/creating-bokeh-backgrounds>.
- [10] Craig Hull, "Step by Step Guide to Beautiful Bokeh," *Expert Photography*, <https://expertphotography.com/beautiful-bokeh-effect-photography/>
- [11] Mastin Labs, "Understanding Focal Plane in Photography", <https://www.mastinlabs.com/photoism/articles/understanding-focal-plane-in-photography>, 2018.
- [12] Merklinger, H.M, A technical view of bokeh. *Photo Techniques* 18(3) (1997).
- [13] Todd Vorenkamp, "Understanding Bokeh," <https://www.bhphotovideo.com/explora/photography/tips-and-solutions/understanding-bokeh> (2016).
- [14] Nasim Mansurov, "What is bokeh and how it affects your images", <https://photographylife.com/what-is-bokeh>.
- [15] "Apple Just Released Their Fake Bokeh Portrait Mode to Everyone". *PetaPixel*. 2016-10-24. Retrieved 2017-11-28.
- [16] Simpson, Jayphen (2017-12-11), "How Portrait Mode Works and How It Compares to an \$8,000 Camera". *PetaPixel*. Retrieved 2017-12-11.
- [17] "vivo V5 Plus becomes official with dual front camera, Snapdragon 625". 2017-01-18.
- [18] Hauser, W., Neveu, B., Jourdain, J.-B., Viard, C., and Guichard, F. (2018), Image quality benchmark of computational bokeh. *Electronic Imaging* 2018.
- [19] Harry Guinness, "What is Focal Length in Photography", <https://www.howtogeek.com/353144/what-is-focal-length/>, 2018.
- [20] Mastin Labs, "Understanding Focal Plane in Photography", <https://www.mastinlabs.com/photoism/articles/understanding-focal-plane-in-photography>, 2018.

- [21] Raimo Hartmann, Susana Carregal-Romero, Wolfgang J. Parak, Pilar Rivera_Gil, Chapter 7 - Investigating Nanoparticle Internalization Patterns by Quantitative Correlation Analysis of Microscopy Imaging Data, *Microscopy Imaging Data, Frontiers of Nanoscience, Volume 4, 2012, Pages 181-196.*
- [22] Honor Official Website, "How to Take Bokeh Effect Photos with Honor 10," <https://www.hihonor.com/global/blog/how-to-take-bokeh-effect-photos-with-honor-10/>, 2018
- [23] M. Potmesil and I. Chakravarty, "A lens and aperture camera model for synthetic image generation," *ACM SIGGRAPH Comput. Graph.*, vol. 15, no. 3, pp. 297–305, Aug. 1981.
- [24] A. A. Gershun, "Photometric in Turbid Medium", *State Optics Institute Proceedings*, vol 11, number 99, p. 3-16, 1936
- [25] Emerson, R. C., Bergen, J. R, & Adelson, E. H. (1991). Directionally selective complex cells and the calculation of motion energy in cat visual cortex. *Vision Research*, vol. 32, No.2, pp.203-218,1992
- [26] C. Zhang and T. Chen, "A survey on image-based rendering—representation, sampling and compression," *Signal Process.: Image Commun.*, vol. 19, pp. 1–28, Jan. 2004.
- [27] G. Wu et al., "Light Field Image Processing: An Overview," in *IEEE Journal of Selected Topics in Signal Processing*, vol. 11, no. 7, pp. 926-954, Oct. 2017.doi: 10.1109/JSTSP.2017.2747126
- [28] Epipolar Geometry, https://en.wikipedia.org/wiki/Epipolar_geometry.
- [29] Chamira Udaya Shantha Edussooriya, "Low-Complexity Multi-Dimensional Filters for Plenoptic Signal Processing," University of Victoria, 2015
- [30] J.-X. Chai, X. Tong, S.-C. Chan, and H.-Y. Shum, "Plenoptic sampling," in *Proc. Annu. Conf. Comput. Graph. (SIGGRAPH)*, 2000, pp. 307–318.
- [31] M. Řeřábek and T. Ebrahimi, "New Light Field Image Dataset," 8th International Workshop on Quality of Multimedia Experience (QoMEX), Lisbon, Portugal, 2016.
- [32] S.-C. Pei and S.-B. Jaw, "Two-dimensional general fan-type FIR digital filter design," *Signal Process.*, vol. 37, no. 2, pp. 265–274, May 1994.
- [33] Sanduni U. Premaratne, Chamira U. S. Edussooriya, Chamith Wijenayakey, Len T. Brutonz and Panajotis Agathoklis, "A 4-D Sparse FIR Hyperfan Filter for Volumetric Refocusing of Light Fields by Hard Thresholding," 2018 IEEE 23rd International Conference on Digital Signal Processing (DSP), 2018.
- [34] D. E. Dudgeon and R. M. Mersereau, *Multidimensional Digital Signal Processing*. Englewood Cliffs, NJ: Prentice-Hall, 1984.
- [35] D. G. Dansereau, D. L. Bongiorno, O. Pizarro, and S. B. Williams, "Light field image denoising using a linear 4D frequency-hyperfan allin-focus filter," in *Proc. SPIE Comput. Imag. XI*, vol. 8657, 2013, pp. 86 570P–1–86 570P–14.
- [36] R. Ng, M. Levoy, M. Bredif, G. Duval, M. Horowitz, and P. Hanrahan, "Light field photography with a hand-held plenoptic camera," Stanford Univ., Stanford, CA, Tech. Rep. CTSR 2005-02, 2005.
- [37] D. G. Dansereau, O. Pizarro, and S. B. Williams, "Decoding, calibration and rectification for lenselet-based plenoptic cameras," in *Computer Vision and Pattern Recognition (CVPR)*, 2013, pp. 1027–1034.

Appendix A Function List of Software Tool

- Function:
 - fanfildes.m
 - firrtdfan.m
 - LFDDefaultVal.m
 - LFDisp.m
 - LFDispMouse.m
 - LFDispSetup.m
 - LFDispVidCirc.m
 - LFStore.m
 - test.m
 - test.fig
 - uigetdir2.m
 - volrefocus.m
- File Folder:
 - Pic
- LF Data
 - Dishes1.mat
 - Pillars.mat
 - Swans_1.mat
 - University.mat

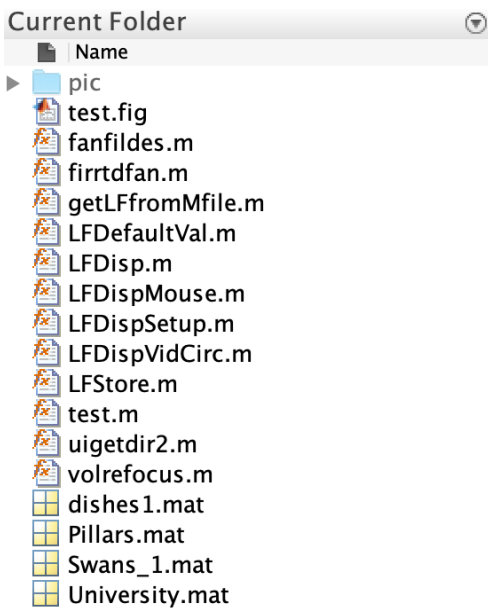


Figure A.1 MATLAB Project Directory

LF data should be placed at the same directory as other function files. When deploying the project on your PC, replace the default path stored in variable named `str` in function `pushbutton2_Callback` with your current `pic` file folder path. Then everything will be ready, and the program starts to run by pressing the run button in `test.m` file.

Appendix B Derivation of the Spectrum of a Lambertian Point Source at a Constant Depth

According to [29], the 4-D continuous-domain Fourier transform of $l_{4C}(x, y, u, v)$ given in (2.6) can be expressed as

$$\begin{aligned}
 L_{4C}(\boldsymbol{\Omega}) &= \int_{x,y,u,v=-\infty}^{\infty} \dots \int l_{4C}(\mathbf{x}) e^{-j\boldsymbol{\Omega}^T \mathbf{x}} d\mathbf{x} \\
 &= \int_{x,y,u,v=-\infty}^{\infty} \dots \int l_0(\mathbf{x}) \delta(mx + u + c_x) \times \delta(my + v + c_y) e^{-j\boldsymbol{\Omega}^T \mathbf{x}} d\mathbf{x} \\
 &= l_0 L_{2C}(\Omega_x, \Omega_u) L_{2C}(\Omega_y, \Omega_v), \tag{B.1}
 \end{aligned}$$

where

$$L_{2C}(\Omega_x, \Omega_u) = \iint_{x,u=-\infty}^{\infty} \delta(mx + u + c_x) e^{-j(\Omega_x x + \Omega_u u)} dudx \tag{B.2a}$$

$$L_{2C}(\Omega_y, \Omega_v) = \iint_{y,v=-\infty}^{\infty} \delta(my + v + c_y) e^{-j(\Omega_y y + \Omega_v v)} dvdy \tag{B.2b}$$

$$\boldsymbol{\Omega} = [x, y, u, v] \tag{B.2c}$$

Now we evaluate (B.2a) as

$$\begin{aligned}
 L_{2C}(\Omega_x, \Omega_u) &= \iint_{x,u=-\infty}^{\infty} \delta(mx + u + c_x) e^{-j(\Omega_x x + \Omega_u u)} dudx \\
 &= \int_{x=-\infty}^{\infty} e^{-j(\Omega_x x + \Omega_u (-mx - c_x))} dx \\
 &= e^{-j\Omega_u c_x} \int_{x=-\infty}^{\infty} e^{-j(\Omega_x - m\Omega_u)x} dx \\
 &= 2\pi \delta(\Omega_x - m\Omega_u) e^{j\Omega_u c_x} \tag{B.3}
 \end{aligned}$$

Here, we have used the fact that $\delta(mx + u + c_x) \neq 0$ only when $mx + u + c_x = 0$. Similarly, $L_{2C}(\Omega_y, \Omega_v)$ can be obtained as

$$L_{2C}(\Omega_y, \Omega_v) = 2\pi \delta(\Omega_y - m\Omega_v) e^{j\Omega_v c_y} \tag{B.4}$$

By substituting (A.3) and (A.4) into (A.1), $L_{4C}(\boldsymbol{\Omega})$ can be obtained as

$$L_{4C}(\boldsymbol{\Omega}) = 4\pi^2 l_0 \delta(\Omega_x - m\Omega_u) \delta(\Omega_y - m\Omega_v) e^{j(\Omega_u c_x + \Omega_v c_y)} \tag{B.5}$$